

SN 2012ec: mass of the progenitor from PESSTO follow-up of the photospheric phase.

C. Barbarino^{1,2}, M.Dall’Ora², M.T. Botticella², M. Della Valle^{2,3}, L. Zampieri⁴, M.L. Pumo⁴, A. Jerkstrand⁵, J.R. Maund⁶, S. Benetti⁴, N. Elias-Rosa⁴, M. Fraser¹⁷, A. Gal-Yam⁷, M. Hamuy^{15,16}, C. Inserra⁵, C. Knapic⁸, A.P. LaCluyze¹⁴, M. Molinaro⁸, P. Ochner⁴, A. Pastorello⁴, G. Pignata^{9,15}, D.E. Reichart¹⁴, C. Ries¹², A. Riffeser¹², B. Schmidt¹⁰, M. Schmidt¹², R. Smareglia⁸, S.J. Smartt⁵, K. Smith⁵, J. Sollerman¹⁸, M. Sullivan¹¹, L. Tomasella⁴, M. Turatto⁴, S. Valenti¹³, O. Yaron⁷ and D. Young⁵.

¹*Dip. di Fisica and ICRA, Sapienza Università di Roma, Piazzale Aldo Moro 5, I-00185 Rome, Italy*

²*INAF- Osservatorio Astronomico di Capodimonte, Salita Moiariello 16, 80131 Napoli, Italy*

³*ICRANet-Pescara, Piazza della Repubblica 10, I-65122 Pescara, Italy*

⁴*INAF- Osservatorio Astronomico di Padova, Vicolo dell’Osservatorio 5, 35122 Padova, Italy*

⁵*Astrophysics Research Centre, School of Mathematics and Physics, Queen’s University Belfast, Belfast BT7 1NN, United Kingdom*

⁶*Department of Physics and Astronomy, University of Sheffield, Sheffield, S3 7RH, United Kingdom*

⁷*Department of Particle Physics and Astrophysics, The Weizmann Institute of Science, Rehovot, 76100 Israel*

⁸*INAF- Osservatorio Astronomico di Trieste, Via Tiepolo Giambattista 11, 34131, Trieste, Italy*

⁹*Departamento de Ciencias Físicas, Universidad Andres Bello, Avda Republica 252, Santiago, Chile*

¹⁰*Research School of Astronomy and Astrophysics, Australian National University, Cotter Road, Weston Creek, ACT 2611, Australia*

¹¹*School of Physics and Astronomy, University of Southampton, Southampton, SO17 1BJ, UK*

¹²*Universitäts-Sternwarte München, Scheinerstr. 1, D-81679 München, Germany*

¹³*Las Cumbres Observatory Global Telescope Network, 6740 Cortona Dr., Suite 102, Goleta, CA 93117, USA*

¹⁴*Department of Physics and Astronomy, University of North Carolina at Chapel Hill, Chapel Hill, NC 27599-3255, USA*

¹⁵*Millennium Institute of Astrophysics (MAS), Santiago, Chile*

¹⁶*Departamento de Astronomía, Universidad de Chile, Casilla 36-D, Santiago, Chile*

¹⁷*Institute of Astronomy, University of Cambridge, Madingley Road, Cambridge, CB3 0HA, UK*

¹⁸*The Oskar Klein Centre, Department of Astronomy, Stockholm University, Albanova, 10691 Stockholm, Sweden*

24 December 2018

ABSTRACT

We present the results of a photometric and spectroscopic monitoring campaign of SN 2012ec, which exploded in the spiral galaxy NGC 1084, during the photospheric phase. The photometric light curve exhibits a plateau with luminosity $L = 0.9 \times 10^{42} \text{ erg s}^{-1}$ and duration ~ 90 days; which is shorter than standard Type IIP supernovae. We estimate the nickel mass $M(^{56}\text{Ni}) = 0.040 \pm 0.015 M_{\odot}$ from the luminosity at the beginning of the radioactive tail of the light curve. The explosion parameters of SN 2012ec were estimated from the comparison of the bolometric light curve and temperature and velocity evolution of the ejecta with predictions from a hydrodynamical model. We derived an envelope mass of $12.6 M_{\odot}$, an initial progenitor radius of $1.6 \times 10^{13} \text{ cm}$ and explosion energy of 1.2 foe. These estimates agree with an independent study of the progenitor star identified in pre-explosion images, for which an initial mass of $M = 14 - 22 M_{\odot}$ was determined. We have applied the same analysis to two other type IIP supernovae (SNe 2012aw and 2012A), and carried out a comparison with the properties of SN 2012ec derived in this paper. We find a reasonable agreement between the masses of progenitor obtained from pre-explosion images and the masses derived from hydrodynamical models. We estimate distances to SN 2012ec with Standardized Candle Method (SCM) and compare with other estimates based on other primary and secondary indicators. SNe 2012A, 2012aw and 2012ec all follow the standard relations for SCM for the use of Type IIP SNe as distance indicators.

Key words: supernovae: general – supernovae: individual: SN 2012ec, SN 2012aw, SN 2012A – supernovae: individual: NGC1084

1 INTRODUCTION

Core-collapse supernovae (CC-SNe) originate from the gravitational collapse of the iron cores formed by massive stars ($M \geq 8 M_{\odot}$) that can not be supported by further exothermal thermonuclear reactions (Iben & Renzini 1983; Woosley et al. 2002). An important sub-class of CC-SNe is represented by Type II-plateau events (SNe IIP) characterized by the presence of hydrogen in their spectra (Filippenko 1997) and a luminosity “plateau” which last for $\sim 80 - 100$ days, after the blue band maximum of the light curve (Barbon et al. 1979). The plateau is powered by the recombination of hydrogen in the SN ejecta. When the recombination ends, the lightcurve sharply drops by several magnitudes in ~ 30 days (e.g. Kasen & Woosley 2009; Olivares et al. 2010). This transition phase is followed by a linear “radioactive tail”, where the light curve is powered by the radioactive decay of ^{56}Co to ^{56}Fe . In this phase the SN luminosity depends on the amount of ^{56}Ni synthesized in the explosion (e.g. Weaver & Woosley 1980). Both theoretical (e.g. Grassberg et al. 1971; Litvinova & Nadezhin 1983; Utrobin & Chugai 2008; Pumo & Zampieri 2011; Bersten et al. 2012) and empirical (e.g. Smartt et al. 2009; Smartt 2009) investigations show that type IIP SNe are generally associated with red supergiants (RSGs). A minor fraction of them (less than 3 – 5%, e.g. Smartt et al. 2009; Pastorello et al. 2012) results from the explosion of a blue supergiant, similar to SN 1987A (Gilmozzi et al. 1987; Kirshner et al. 1987). Theoretical models predict that type IIP SNe are the final fate of progenitors between 8 and $30 M_{\odot}$ (e.g. Heger et al. 2003; Walmswell & Eldridge 2012). Most progenitors identified in high-resolution archival images were found to be RSGs of initial masses between $\sim 8 M_{\odot}$ and $\sim 17 M_{\odot}$. The apparent lack of high-mass progenitors has been dubbed as “RSG problem” (Smartt 2009, *and references therein*). The existence of this discrepancy has been further confirmed by studies on the massive star population in Local Group galaxies, for which RSGs have been found to have masses up to $25 M_{\odot}$ (Massey et al. 2000; Massey et al. 2001). The reason for this lack of detection of massive RSG progenitors is still debated. A possible solution of the RSG problem was presented by Walmswell & Eldridge (2012). They speculate that an underestimation of the luminosity of the RSG SN progenitors (and therefore of their masses) might occur if we neglect the presence of an additional extinction due to dust production in the RSG winds. They estimated a new upper limit for the mass range of $21_{-1}^{+2} M_{\odot}$, which is, within the errors, marginally consistent with the range derived by Smartt (2009). Kochanek et al. (2012) pointed out that the use of interstellar extinction laws may overestimate the effects of extinction. A different approach to estimate the mass of Type IIP SN progenitors is based on the hydrodynamic modelling of the SN evolution. This allows us to determine the ejecta mass, explosion energy, pre-SN radius and Ni mass by performing a simultaneous comparison between the observed and simulated light curves, the evolution of line velocities and the continuum temperature (Litvinova & Nadezhin 1983; Litvinova & Nadezhin 1985; Zampieri 2005; Zampieri 2007). The pre-explosion mass is calculated from the ejecta mass assuming the mass of a neutron star remnant ($1.4 M_{\odot}$) and mass loss through

stellar winds. The hydrodynamic modelling of several well-observed Type IIP SNe (SNe 1997D, Zampieri et al. 1998; 1999em, Elmhamdi et al. 2003; 2003Z, Utrobin et al. 2007 and Spiro et al. 2014; 2004et, Maguire et al. 2010; 2005cs, Pastorello et al. 2009; 2009kf, Botticella et al. 2012) determined higher masses for the progenitors than those derived from the analysis of pre-explosion images. This discrepancy either points to systematic errors in the analysis of pre-explosion images or in the assumptions in the physics of the hydrodynamical modelling (Utrobin 1993; Blinnikov et al. 2000; Chugai & Utrobin 2000; Zampieri et al. 2003; Pastorello et al. 2004; Utrobin 2007, Utrobin et al. 2007; Utrobin & Chugai 2008; Utrobin & Chugai 2009; Pastorello et al. 2009). Another method to estimate the mass of the progenitor is the spectral modeling along the nebular phase (Jerkstrand et al. 2012; Jerkstrand et al. 2014) that is in quite good agreement with the estimate obtained by the analysis of the pre-explosion images.

The astrophysical interest in Type IIP SNe is twofold: 1) observations show that Type IIP SNe are the most common explosions in the nearby Universe (e.g. Cappellaro et al. 1999; Li et al. 2011); and 2) starting from the pioneering suggestion by Kirshner & Kwan (1974), Type IIP SNe have been proposed as robust distance indicators. Two different approaches are used to derive distance measurements of SNe IIP. The theoretical approach is based on spectral modelling like the expanding photosphere method (e.g. Eastman, Schmidt & Kirshner 1996) or the spectral expanding atmosphere method (e.g., Baron et al. 2004). Empirical approaches exploit the observed correlation between the luminosity of a Type IIP SN and its expansion velocity (e.g., the standardized candle method, Hamuy & Pinto 2002) or the steepness of the light curve after the plateau phase (Elmhamdi, Chugai & Danziger 2003). The Hamuy & Pinto (2002) method, refined for example by Nugent et al. (2006), Poznanski et al. (2009), and Olivares et al. (2010), has an intrinsic accuracy of $\sim 10 - 12\%$ (Hamuy & Pinto 2002); slightly larger than the accuracy obtained for Type Ia SNe (e.g. Tammann & Reindl 2013). Type IIP SNe can, importantly, be observed out to cosmological distances (e.g. Nugent et al. 2006); with the advantage of being that they arise a homogenous progenitor population. The Hamuy & Pinto (2002) method can, therefore, be used as an independent health check of the SN Ia-based distance scale.

The main goal of this paper is to present the results of our photometric and spectroscopic monitoring campaign of SN 2012ec, which exploded in NGC 1084. The early data were collected via the Large Program “Supernova Variety and Nucleosynthesis Yields” (PI S. Benetti). A substantial fraction of the data has been collected via the ESO Public Survey PESSTO¹ (“Public ESO Spectroscopic Survey of Transient Objects”, PI S.J. Smartt). The observations of SN 2012ec were analysed in conjunction with the hydrodynamical codes described in Pumo et al. (2010) and Pumo & Zampieri (2011), and information on the progenitor obtained from high-resolution pre-explosion images. The same analysis has already performed for two other type

¹ www.pessto.org

IIP SNe: SN 2012A (Tomasella et al. 2013; Roy et al. 2014) and SN 2012aw (Fraser et al. 2012; Bayless et al. 2013; Bose et al. 2013; Dall’Ora et al. 2014). This allows us to carry out an homogeneous comparative study of these three SNe, and to identify possible systematic discrepancies in the estimate of the masses of the progenitors derived from different techniques.

The paper is organized as follows: in Section 2 we present the discovery and the detection of the progenitor of SN 2012ec; in Section 3 we discuss the properties of the host galaxy, the distance and the extinction; in Section 4 we present the optical and near-infrared (NIR) photometric evolution of SN 2012ec, and compare its colour evolution and bolometric light curve with those of other Type IIP SNe. In Section 5 we present the optical and NIR spectroscopic observations. In Section 6 we discuss the results of the modeling of the data and in Section 7 we present a detailed comparison of SN 2012ec with the Type IIP SNe SN 2012A and SN 2012aw. In Section 8 we consider these three SNe in the context of the standardised candle method and in Section 9 we discuss our results.

2 DISCOVERY AND PROGENITOR DETECTION

SN 2012ec was discovered by Monard (2012) in the almost face-on ($i = 57^\circ$, Moiseev 2000) spiral galaxy NGC 1084 on 2012 August 11.039 UT (MJD=56150.04). Childress et al. (2012) classified SN 2012ec as a very young age type IIP SN, probably a few days after the explosion. In Fig. 1 we show this early spectrum of SN 2012ec (collected on 2012, August 13 with WiFeS, MJD = 56152.2), compared with SN 2006bp (Quimby et al. 2007) at five different epochs. The spectrum of SN 2012ec is very similar to those of SN 2006bp (Quimby et al. 2007) obtained at 8 and 10 days after the explosion, implying that the SN was observed at $\sim +9$ days post-explosion and an explosion epoch of ~ 7 days before the discovery. We explicitly note that our estimate is slightly different from the one given by Maund et al. (2013), who estimated the explosion date at < 6 days before the discovery by comparison with spectra of SN 1999em. The explosion epoch of SN 2006bp is much more tightly constrained than that of SN 1999em, because it is based on the detection of shock breakout (Nakano 2006; Quimby et al. 2007). We adopt, therefore, a conservative constraint on the explosion date of 7 ± 2 days prior to discovery and define the zero phase as our estimated explosion epoch of MJD = 56143.0.

Maund et al. (2013) identified a progenitor candidate in pre-explosion Hubble Space Telescope (HST) images. Photometry of the progenitor candidate was compared with synthetic photometry of MARCS spectral energy distributions (SED) (Gustafsson et al. 2008), which suggested that the progenitor of SN 2012ec was a RSG with an initial mass in the range $14 - 22 M_\odot$.

3 HOST GALAXY, DISTANCE AND EXTINCTION

The SN is located $0.7''$ E and $15.9''$ N of the nucleus of the host galaxy NGC 1084 (see Fig 2). Details of NGC 1084 are

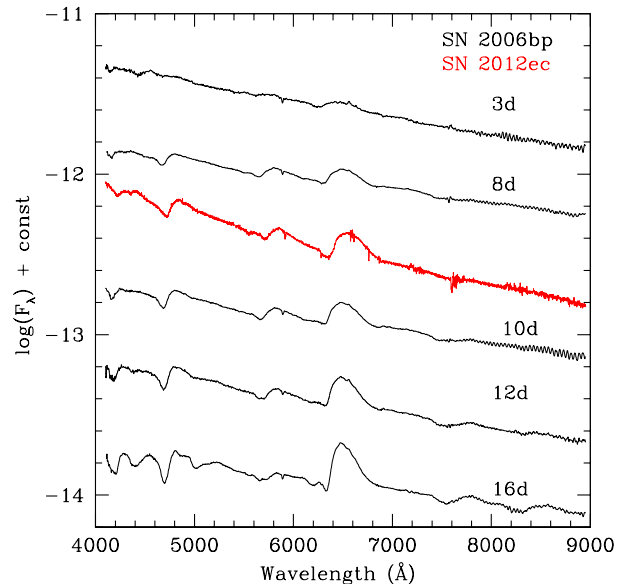


Figure 1. Comparison between a very early spectrum of SN 2012ec and 5 spectra of SN 2006bp from day 3 to 16.

presented in Table 1. NGC 1084 previously hosted 4 known SNe: the Type IIP SN 2009H (Li et al. 2009), the Type II SNe 1998dl (King et al. 1998) and 1996an (Nakano et al. 1996), and the Type Ia SN 1963P (Kowal 1968).

The distances available in the literature for NGC 1084 are principally based on the Tully-Fisher relation, and we adopt the value $\mu = 31.19 \pm 0.13$ mag, available in the Extragalactic Distance Database² (Tully et al. 2009).

The Galactic reddening towards SN 2012ec was estimated from the Schlafly & Finkbeiner (2011) dust maps to be $E(B - V) = 0.024$ mag. The internal reddening in NGC 1084 was derived using the measured equivalent widths (EW) of NaI D (5889, 5895 Å), observed in a low-resolution spectrum at 19 days. The measured value was $EW(\text{NaI D}) = 0.8 \pm 0.3$ Å from which we obtained $E(B - V) = 0.12^{+0.15}_{-0.12}$ mag using the Poznanski et al. (2012) calibration and $E(B - V) = 0.11$ mag using the Turatto et al. (2003) calibration. These two values are in good agreement and we adopt $E(B - V) = 0.12^{+0.15}_{-0.12}$ mag for the host galaxy extinction.

Finally, we transformed both Galactic and host reddening in selective absorption by adopting the Assuming a Cardelli et al. (1989) reddening law ($R_V = 3.1$) we estimate the total V -band extinction towards SN 2012ec to be $A_V = 0.45$ mag.

4 PHOTOMETRIC EVOLUTION

4.1 Data sample and reduction

A photometric and spectroscopic monitoring campaign for SN 2012ec, at optical and NIR wavelengths, was conducted over a period 153 days, covering 77 epochs from 11 to 164

² Extragalactic Distance Database, <http://edd.ifa.hawaii.edu/>

Table 1. Properties of NGC 1084.

α (2000)	$2^h 43^m 32.091$
δ (2000)	$-07^\circ 47' 16.76''$
morphological type	SA(s)d
z	0.004693 ± 0.000013
μ	31.19 ± 0.13 mag
v_{Hel}	1407 ± 4 km s $^{-1}$
$E(B - V)_{\text{Galactic}}$	0.024 mag
$E(B - V)_{\text{host}}$	0.12 mag

days post-explosion, using multiple observing facilities. Additional data collected in the nebular phase will be published in a companion paper (Jerkstrand et al. 2014, *in prep*).

BVRI Johnson-Cousins data were collected with: the 2.0m Liverpool Telescope (LT, Canary Islands, Spain) equipped with the IO:O camera (*BV*, 21 epochs); the 3.58m ESO New Technology Telescope (NTT, La Silla, Chile) equipped with the EFOSC2 (ESO Faint Object and Spectrograph Camera) camera (*BVRI*, 9 epochs); the 1.82m Copernico telescope (Asiago, Italy) equipped with the AFOSC Asiago Faint Object Spectrograph and Camera (*BVRI*; 3 epochs); the 0.6m ESO TRAnsiting Planets and PlanetsImals Small Telescope (TRAPPIST, La Silla, Chile), equipped with TRAPPISTCAM (*BVR*, 4 epochs); and the the array of 0.41m Panchromatic Robotic Optical Monitoring and Polarimetry Telescopes (PROMPT, Cerro Tololo, Chile), equipped with Apogee U47p cameras, which employ the E2V CCDs (*BVRI*, 21 epochs).

ugriz images were collected with: the LT equipped with the IO:O camera (*uriz* 21 epochs); the ESO NTT Telescope equipped with EFOSC2 (*ugriz*, 3 epochs); the PROMPT telescopes (*griz*, 19 epochs); and the 0.4m telescope at the Wendelstein Observatory (Mount Wendelstein, Germany), equipped with a ST-10 CCD camera (*gri*, 7 epochs).

JHK_s observations were acquired with the ESO NTT telescope, equipped with the SOFI (Son Of ISAAC) camera (8 epochs).

A summary of the characteristics of the instruments and telescopes used for photometric follow up are presented in Table 2.

Data were pre-reduced by the instruments pipelines, where available, or following the standard procedures (bias, overscan and flat-field corrections, trimming) in the IRAF³ environment. In particular, the NIR images were pre-reduced by means of an IRAF-based custom pipeline using the XDIMSUM IRAF package (Coppola et al. 2011), which conducts the background subtraction using a two-step technique based on a preliminary guess of the sky background and on a careful masking of unwanted sources in the sky images.

Johnson-Cousins *BVRI* calibrated magnitudes of 18 reference stars were obtained by averaging their photometry obtained on 12 photometric nights, in conjunction with observations of Landolt (1992) standard star fields. *ugriz* calibrated photometry for 17 reference stars were obtained on

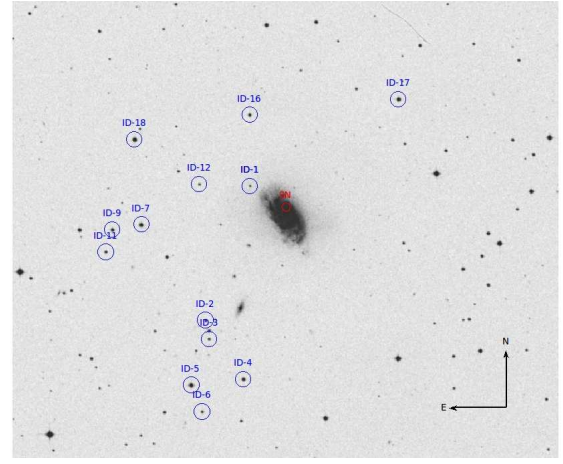


Figure 2. An image of SN 2012ec and the host galaxy NGC 1084, acquired with the Liverpool Telescope and the IO:O camera. The field of view is 14.5×14.5 arcmin². Reference stars are circled and labeled (see Tables 3 and 4).

11 photometric nights with the LT and the NTT telescopes, on the in conjunction with observations of Smith et al. (2002) *u'g'r'i'z'* standard star fields. Finally, calibrated NIR 2MASS *JHK* photometry was obtained for 5 reference stars, for which 2MASS (Skrutskie et al. 2006) photometry was available. We did not correct NIR magnitudes for the colour terms, since they are generally very small in the NIR bands (e.g. Carpenter 2001). Our adopted reference stars showed no clear signs of variability.

The Johnson-Cousins *BVRI* and NIR photometry is reported in Vega magnitudes, while the *ugriz* photometry is reported in the AB magnitude system. The host galaxy and the SN position are shown in Fig. 2, along with the local sequence stars adopted for the photometric calibration. The calibrated photometry for the local sequence stars is reported in Tables 3 and 4.

Photometric measurements were carried out with the QUBA pipeline (Valenti et al. 2011), which performs DAOPHOT-based (Stetson 1987) point-spread-function (PSF) fitting photometry on the SN and on the selected reference stars. Since SN 2012ec is embedded in a spiral arm of the host galaxy, the background was estimated with a polynomial model. We performed empirical tests for the best background subtraction, and in most cases we found that a 4th-order polynomial model of the background gave satisfactory results, due to the high S/N ratio of the SN in these images. Only for the last few epochs the S/N ratio of the SN too low to prohibit satisfactory removal of the local background. We note, however, that even a subtraction of template image would probably yield a significant improvement, as in these cases the flux of the SN was only few tens of counts above the local background. An estimate of the photometric errors was automatically performed by the pipeline using artificial stars experiments.

The photometric measurements of the SN in the *BVRI*, *u'g'r'i'z'* and in the *JHK* filter systems are reported in Table 5.

³ IRAF is distributed by the National Optical Astronomical Observatory, which is operated by the Association of Universities for Research in Astronomy, Inc., under cooperative agreement with the National Science Foundation.

Table 2. Summary of the characteristics of the instruments used during the photometric follow up.

Telescope	Camera	Pixel scale [arcsec/pix]	Field of view [arcmin]	Filters ^a	# of epochs
NTT (3.58m)	EFOSC2	0.24	4×4	$B, V, R; u, g, r, i$	12
NTT (3.58m)	SOFI	0.28	5×5	J, H, K_s	8
LT (2.0m)	IO:O	0.15	10×10	$B, V: u, r, i, z$	21
PROMPT (0.41m)	APU9	0.59	11×11	$B, V, R, I; g, r, i, z$	21
CAO (1.82m)	AFOSC	0.46	8×8	$B, V, R; i$	3
SAO (0.97m)	SBIG	0.86	57×38	R	1
WOT (0.4m)	SBIG ST-10 XME	0.44	16×10	g, r, i	7
TRAPPIST (0.60m)	TRAPPISTCAM	0.65	27×27	B, V, R	4

NTT = New Technology Telescope with the optical camera ESO Faint Object Spectrograph and Camera EFOSC2 and with the Near-Infrared Camera Son of ISAAC (SOFI); LT = the Liverpool Telescope (LT) with the optical CCD CAMERA IO:O; PROMPT = Panchromatic Robotic Optical Monitoring and Polarimetry Telescopes; CAO = the Copernico telescope at Asiago Observatory with the Asiago Faint Object Spectrograph and Camera (AFOSC); SAO = the Schmidt telescope at the Asiago Observatory; WOT = the 40 cm telescope at the Wendelstein Observatory; TRAPPIST = TRAnsit Planets and PlanetesImals Small Telescope.

^a The NTT and CAO i filter is Gunn.

Table 3. Positions and photometry of the local sequence reference stars in the $BVRI$ and in the $u'g'r'i'z'$ systems.

# id	$\alpha_{J2000.0}$ (deg)	$\delta_{J2000.0}$ (deg)	B mag	V mag	R mag	I mag	u' mag	g' mag	r' mag	i' mag	z' mag
1	41.5216674	-7.5597940	17.98 (0.02)	16.88 (0.02)	16.19 (0.02)	15.53 (0.03)	19.85 (0.02)	17.48 (0.04)	16.41 (0.01)	16.01 (0.02)	15.86 (0.01)
2	41.5496917	-7.6416869	16.84 (0.02)	15.97 (0.02)	15.46 (0.02)	14.93 (0.03)	18.27 (0.02)	16.43 (0.02)	15.67 (0.02)	15.38 (0.01)	15.32 (0.02)
3	41.5474764	-7.6530580	17.14 (0.02)	16.28 (0.02)	15.81 (0.02)	15.32 (0.02)	18.45 (0.06)	16.71 (0.03)	16.04 (0.02)	15.78 (0.01)	15.72 (0.01)
4	41.5265649	-7.6778087	15.58 (0.02)	14.95 (0.02)	14.66 (0.02)		16.48 (0.03)	15.25 (0.02)	14.80 (0.02)	14.64 (0.02)	14.65 (0.01)
5	41.5589242	-7.6811761	14.27 (0.02)	13.52 (0.02)	13.23 (0.02)		15.18 (0.02)	13.91 (0.02)	13.31 (0.02)	13.05 (0.02)	12.94 (0.01)
6	41.5522025	-7.6973300	17.01 (0.02)	16.00 (0.02)	15.43 (0.02)		18.82 (0.05)	16.55 (0.03)	15.62 (0.02)	15.30 (0.02)	15.18 (0.01)
7	41.5886692	-7.5829251	14.62 (0.01)	14.07 (0.01)	13.84 (0.02)		15.36 (0.03)	14.49 (0.02)	13.98 (0.01)	13.86 (0.02)	13.87 (0.01)
9	41.6065545	-7.5858940	15.16 (0.01)	14.42 (0.01)	14.08 (0.02)		16.11 (0.02)	15.03 (0.03)	14.25 (0.02)	14.04 (0.02)	14.01 (0.01)
11	41.6108998	-7.5996059	16.99 (0.01)	16.36 (0.01)	16.04 (0.02)		17.64 (0.02)	16.66 (0.03)	16.21 (0.01)	15.99 (0.02)	15.97 (0.02)
12	41.5528922	-7.5585795	18.32 (0.02)	16.83 (0.02)	15.93 (0.02)	14.73 (0.02)	20.12 (0.05)	17.65 (0.01)	16.19 (0.01)	15.24 (0.02)	14.90 (0.02)
16	41.5215760	-7.5167457	16.06 (0.01)	15.26 (0.01)	14.90 (0.02)	14.48 (0.01)	17.25 (0.04)	15.64 (0.03)	15.10 (0.02)	14.93 (0.02)	14.86 (0.01)
17	41.4300180	-7.5076398	14.74 (0.01)	14.08 (0.01)	13.81 (0.02)		14.92 (0.02)	14.43 (0.02)	14.18 (0.02)	13.92 (0.01)	13.95 (0.01)
18	41.5925440	-7.5310037	16.06 (0.01)	13.76 (0.01)	14.90 (0.02)						

4.2 Data analysis

The photometric evolution of SN 2012ec in the $BVRI$, JHK and in the $u'g'r'i'z'$ filter systems is shown in Fig. 3.

SN 2012ec was already on the plateau in the V, R, I, r', i' and z' bands by +13 days. The average absolute magnitude, in the different bands, during the plateau phase was $M_V = -16.54$ mag, $M_R = -16.75$ mag, $M_I = -16.96$ mag, $M_{r'} = -16.80$ mag, $M_{i'} = -16.93$ mag and $M_{z'} = -17.08$ mag. The plateau lasted almost 90 days in R, I, r', i', z' , almost 80 days in V ; shorter than the usual duration of the plateau of standard Type IIP SNe (e.g. SN 2004et 100 days Maguire et al. 2010, SN 2012aw 100 days Dall'Ora et al. 2014, see also Arcavi et al. 2012). SN 2012ec began to fall from the plateau at $\sim +90$, while the photospheric phase from the observed spectroscopic evolution (see Sect. 5.2) lasted until 160 days. The decline in the light curve of SN 2012ec, from the plateau to the radioactive decay tail, lasted ~ 30 days, decreasing 1.5 mag in r', i', V bands, of 1 mag in I bands and of 1.3 mag in the z' band. A list of the main characteristics of the light curve, for each filter, is reported in Table 6.

The NIR light curve exhibits a plateau of duration $\sim 90 - 100$ days, which subsequently drops over a period of 40 days by 1.3 mag in J band, 1.1 mag in the H band and 1.2 mag in the K band. This behaviour is similar to the one

observed in other Type IIP SNe (see for example, SN 2012A, Tomasella et al. 2013; SN 2012aw Dall'Ora et al. 2014).

The $B - V$, $V - R$ and $V - K$ colours evolution of SN 2012ec are shown in Fig. 4. The $B - V$ presents a clear trend in the first 50 days and then it becomes almost constant. It goes from an initial $B - V \sim 0$ mag then rises to ~ 1 mag and stays constant at around this value until day 160. The $V - R$ shows a steady increase, in the range 0 – 1 mag. The $V - K$ starts from 0.7 mag and increase slowly till ~ 1 mag at ~ 100 days, then it shows a further increase from ~ 1 to ~ 1.9 mag in the period 100 – 130 days. The colour evolutions of SN 2012ec are similar to these of other type IIP SNe (e.g. SN 2004et, Maguire et al. 2010; SN 1999em, Elmhamdi et al. 2003; SN 2009bw, Inserra et al. 2012).

4.3 Bolometric light curve and ^{56}Ni mass

A pseudo-bolometric light curve was calculated by integrating over the optical and NIR photometry. The estimated $u'Bg'Vr'Ri'Iz'JHK$ apparent magnitudes have been converted into monochromatic fluxes at the effective wavelength for each filter, and then corrected for extinction (Sect. 3). The resulting Spectral Energy Distribution (SED) was been integrated over the entire wavelength range, assuming zero flux at the limits. The estimation of the flux was performed at only those phases for which V band observa-

Table 4. Positions and photometry of the local sequence reference stars in the 2MASS *JHK* system.

Star ID	$\alpha_{J2000.0}$ (deg)	$\delta_{J2000.0}$ (deg)	<i>J</i> (mag)	<i>H</i> (mag)	<i>K</i> (mag)
1	41.5216674	-7.5597940	14.82 (0.04)	14.08 (0.05)	13.94 (0.05)
2	41.5496917	-7.6416869	14.32 (0.03)	13.87 (0.04)	13.73 (0.05)
3	41.5474764	-7.6530580	14.71 (0.04)	14.35 (0.05)	14.14 (0.06)
12	41.5528922	-7.5585795	13.63 (0.03)	13.01 (0.03)	12.81 (0.03)

Table 5. Optical photometry in Johnson-Cousins filters, in *u'g'r'i'z'* bands and NIR photometry calibrated to the 2MASS system, with associated errors in parentheses. We constrain the explosion epoch to *MJD* = 56143.0.

Date	<i>MJD</i>	<i>B</i> (mag)	<i>V</i> (mag)	<i>R</i> (mag)	<i>I</i> (mag)	<i>u'</i> (mag)	<i>g'</i> (mag)	<i>r'</i> (mag)	<i>i'</i> (mag)	<i>z'</i> (mag)	<i>J</i> (mag)	<i>H</i> (mag)	<i>K</i> (mag)
20120814	56154.22	14.99 (0.02)	14.81 (0.02)			15.02 (0.04)		14.78 (0.02)	14.91 (0.02)				
20120815	51155.22	14.99 (0.04)	14.86 (0.04)			15.09 (0.02)		14.81 (0.02)	14.91 (0.02)				
20120817	56157.59	15.12 (0.06)	14.90 (0.06)	14.74 (0.06)	14.55 (0.05)								
20120818	56158.23	15.10 (0.03)	14.87 (0.03)			15.28 (0.05)		14.82 (0.01)	14.94 (0.01)				
20120819	56158.34	15.15 (0.06)	14.95 (0.05)	14.73 (0.06)	14.53 (0.03)			14.84 (0.05)	14.86				
20120820	56159.31	15.29 (0.05)	14.92 (0.04)	14.62 (0.05)	14.53 (0.05)		15.05 (0.07)	14.78 (0.03)	14.86 (0.06)				
20120821	56160.30	15.18 (0.07)	14.86 (0.06)	14.65 (0.03)	(14.61 (0.06))		15.13 (0.10)	14.81 (0.04)	14.89 (0.04)	14.92 (0.05)			
20120826	56165.28	15.47 (0.05)	14.93 (0.04)	14.64 (0.04)		16.35 (0.04)	15.25 (0.08)	14.80 (0.03)	14.87 (0.03)	14.92 (0.03)	14.24 (0.02)	14.04 (0.02)	13.91 (0.02)
20120828	56168.20	15.55 (0.02)	15.02 (0.02)			16.52(0.06)		14.85 (0.02)	14.93 (0.02)				
20120831	56171.08	15.67 (0.06)	14.98 (0.06)			16.69 (0.08)		14.81 (0.02)	14.94 (0.02)				
20120902	56173.09	15.76 (0.04)	14.99 (0.04)			16.98 (0.06)		14.85(0.02)	14.92 (0.02)				
20120905	56176.13	15.76 (0.04)	15.00 (0.05)	14.65 (0.06)	14.62 (0.06)	17.05 (0.07)		14.84 (0.03)	14.86 (0.03)	14.89 (0.03)			
20120909	56179.34	15.90 (0.06)	15.10 (0.06)	14.78 (0.04)	14.45 (0.02)		15.54 (0.02)		14.92		14.11 (0.03)	13.89 (0.03)	13.82 (0.03)
20120910	56180.92	15.95 (0.04)	15.14 (0.03)	14.76 (0.01)	14.51 (0.01)								
20120911	56181.59	16.05 (0.02)	15.15 (0.02)	14.79 (0.03)	14.53 (0.03)								
20120916	56186.20	16.06 (0.07)	15.10 (0.06)	14.75 (0.04)	14.49 (0.02)	15.51 (0.04)	14.89 (0.04)	14.87 (0.02)	14.85 (0.03)				
20120920	56190.24		15.12 (0.03)		14.42 (0.05)			14.89 (0.03)	14.85 (0.03)	14.87 (0.03)			
20120923	56194.87	16.15 (0.02)	15.10 (0.02)	14.78 (0.01)	14.45 (0.01)								
20120924	56195.23										14.08 (0.03)	13.89 (0.03)	13.75 (0.03)
20120926	56196.20	16.16 (0.06)	15.00 (0.05)	14.72 (0.03)		17.96 (0.09)	15.56 (0.03)	14.81 (0.03)	14.81 (0.03)	14.78 (0.03)			
20120929	56199.29		15.02 (0.03)	14.74 (0.03)	14.36 (0.01)			14.88 (0.02)	14.81 (0.02)	14.79 (0.02)			
20121001	56202.01	16.19 (0.05)	15.11 (0.05)			17.98 (0.11)		14.89 (0.02)	14.80 (0.03)	14.82 (0.02)			
20121002	56202.20	16.28 (0.04)	15.04 (0.04)	14.74 (0.04)	14.40 (0.02)		15.61 (0.06)	14.93 (0.05)	14.84 (0.04)	14.85 (0.04)			
20121004	56204.21	16.33 (0.04)	15.12 (0.03)	14.73 (0.03)	14.43 (0.02)	18.07 (0.14)	15.71 (0.04)	14.90 (0.03)	14.84 (0.02)	14.84 (0.02)			
20121007	56208.04	16.23 (0.08)	15.11 (0.08)			18.07 (0.18)		14.85 (0.02)	14.78 (0.02)	14.81 (0.03)			
20121010	56211.05	16.35 (0.04)	15.16 (0.04)			18.26 (0.10)	15.68 (0.03)	14.89 (0.01)	14.83 (0.01)	14.85 (0.02)			
20121012	56212.19	16.46 (0.06)	15.22 (0.07)	14.78 (0.03)	14.41 (0.02)			14.94 (0.02)	14.79 (0.03)	14.87 (0.03)			
20121016	56216.35										14.05 (0.03)	13.80 (0.03)	13.59 (0.03)
20121017	56217.15	16.50 (0.07)	15.22 (0.06)					14.95 (0.03)	14.89 (0.03)	14.77 (0.04)			
20121019	56220.42	16.63 (0.05)	15.28 (0.05)	14.77 (0.04)	14.41 (0.03)								
20121020	56221.06	16.58 (0.03)	15.36 (0.03)	14.8 (0.1)	14.43 (0.02)	18.68 (0.08)		14.96 (0.02)	14.86 (0.02)	14.92 (0.02)			
20121022	56223.52							15.00 (0.02)	14.85 (0.03)				
20121024	56226.45						15.99 (0.06)	15.01 (0.02)	14.91 (0.03)				
20121101	56232.13	16.79 (0.09)	15.47 (0.08)	14.95 (0.04)	14.59 (0.02)		16.00 (0.06)	15.15 (0.03)		15.05 (0.03)			
20121106	56237.12		15.63 (0.03)	15.04 (0.03)	14.67 (0.03)		16.2 (0.1)	15.26 (0.02)	15.15 (0.02)	15.16 (0.02)	14.35 (0.06)	14.12 (0.06)	14.04 (0.04)
20121111	56242.13	17.1 (0.1)	15.85 (0.08)	15.26 (0.03)	14.85 (0.03)		16.38 (0.06)	15.39 (0.02)	15.29 (0.02)	15.26 (0.03)			
20121114	56245.20										14.58 (0.03)	14.34 (0.03)	14.28 (0.03)
20121115	56246.96	17.4 (0.1)	16.09 (0.10)					15.63 (0.02)	15.47 (0.02)	15.43 (0.02)			
20121117	56248.14		16.26 (0.04)	15.57 (0.05)	15.15 (0.04)								
20121119	56250.19	17.82 (0.09)	16.49 (0.08)	15.85 (0.05)	15.37 (0.05)		17.24 (0.05)	16.00 (0.02)	15.89 (0.02)	15.74 (0.03)			
20121122	56253.08	17.95 (0.10)	17.16 (0.10)	16.36 (0.07)	15.63 (0.05)		17.45 (0.10)	16.32 (0.03)	16.29 (0.03)	16.12 (0.12)			
20121204	56266.14										15.73 (0.06)	15.27 (0.08)	15.40 (0.06)
20121205	56266.93	18.5 (0.2)	17.3 (0.2)					16.65 (0.07)	16.51 (0.07)	16.40 (0.06)			
20121207	56268.94	18.60 (0.15)	17.40 (0.15)					16.80(0.1)	16.6 (0.1)	16.50 (0.06)			
20121209	56270.95	18.70 (0.13)	17.50 (0.13)					16.9 (0.1)	16.7 (0.1)	16.6 (0.1)			
20121216	56277.99							17.0 (0.1)	16.9 (0.1)	16.8 (0.1)			
20121220	56282.94	18.8 (0.2)	17.7 (0.2)	16.9 (0.2)									
20121221	56283.10										15.83 (0.03)	15.41 (0.03)	15.47 (0.03)
20121228	56290.00	19 (0.2)	17.9 (0.2)					17.1 (0.1)	17.1 (0.1)	16.9 (0.1)			
20130110	56302.81	19.15 (0.30)	18.0 (0.3)					17.2 (0.1)	17.2 (0.1)	17.0 (0.1)			
20130112	56305.66		18.0 (0.3)	17.15 (0.30)	16.75 (0.30)								

tions were available. If photometry for other bands was not available, the magnitudes were estimated at these phases by interpolating the values from photometry acquired on adjacent nights. The final integrated fluxes were converted to luminosity through application of the adopted distance modulus. The pseudo-bolometric light curve of SN 2012ec is shown in Fig. 5. The luminosity at the first epoch for which the calculation could be conducted (14 days) was $L = 1.4 \times 10^{42} \text{ erg s}^{-1}$; this can be considered a lower limit for the bolometric luminosity. The SN luminosity reaches the plateau by day 20 ($L = 0.9 \times 10^{42} \text{ erg s}^{-1}$), which then begins to significantly decrease at 91 days to the tail at day 130, with a luminosity of $L = 0.1 \times 10^{42} \text{ erg s}^{-1}$.

A comparison of pseudo-bolometric light curve of SN 2012ec with other Type IIP SNe demonstrates a similar

behaviour (e.g. SN 2012A Tomasella et al. 2013; SN 2012aw Dall'Ora et al. 2014; SN 2009kf Botticella et al. 2012 and SN 2005cs Pastorello et al. 2009). The pseudo-bolometric light curve of SN 2012ec shows that the luminosity on the plateau is lower than the high luminosity of SN 2012aw and of SN 2009kf, the latter, being so luminous can be considered as an upper limit. SN 2012ec also shows to have a shorter plateau respect to the more luminous SNe. Instead SN 2012ec is more luminous than SN 2012A and SN 2005cs but the latter shows to be with a shorter plateau.

We estimated the ^{56}Ni mass synthesised during the explosion, by comparing the luminosity of SN 2012ec with that of SN 1987A at similar late epochs. Assuming a similar γ -ray deposition fraction, the mass of ^{56}Ni was calculated using the relation of Bouchet et al. (1991):

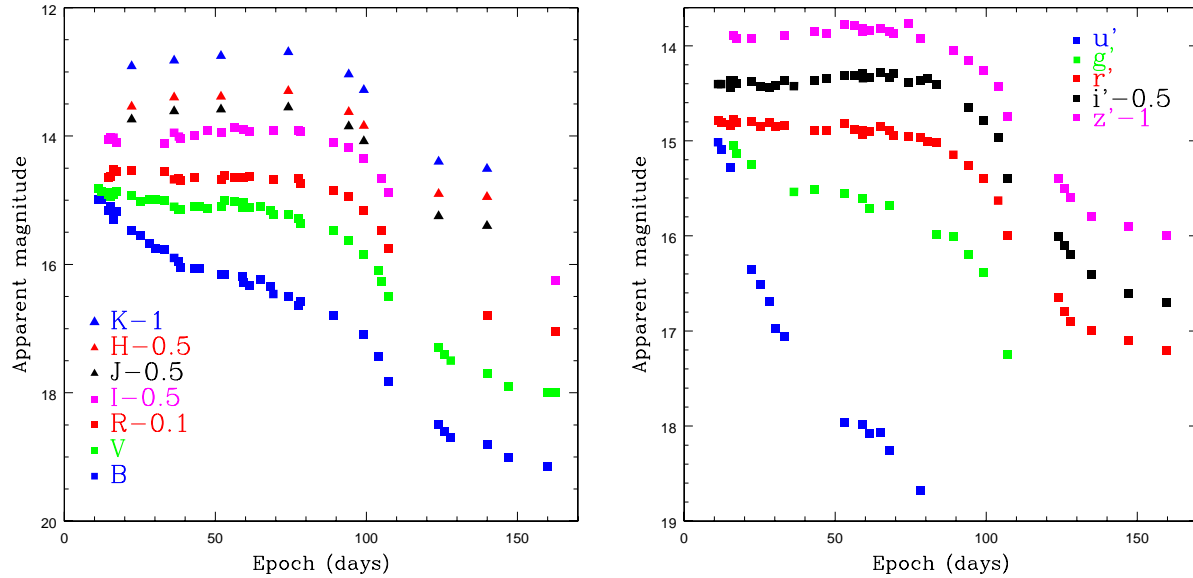


Figure 3. Left panel: photometric evolution of SN2012ec in the Johnson-Cousins *BVRI* and *JHK* filters. Right panel: photometric evolution of SN2012ec in the *u'gr'iz'* filters. A shift has been applied for clarity.

Table 6. Epochs and apparent magnitudes of light curve during the plateau in the *VRIR'iz'* bands.

	V	R	I	<i>r'</i>	<i>i'</i>	<i>z'</i>	J	H	K
	mag	mag	mag	mag	mag	mag	mag	mag	mag
m_{plat}^a	15.10 (0.02)	14.78 (0.01)	14.45 (0.01)	14.89 (0.03)	14.85 (0.03)	14.87 (0.03)	14.08 (0.03)	13.89 (0.03)	13.75 (0.03)
M_{plat}^a	-16.54 (0.17)	-16.75 (0.17)	-16.96 (0.17)	-16.80 (0.18)	-16.93 (0.18)	-17.08 (0.18)	-17.24 (0.18)	-17.38 (0.18)	-17.49 (0.18)

^a Plateau phase refers to 59 days after the explosion at $MJD = 56202.0$

$$M(^{56}\text{Ni})_{12ec} = M(^{56}\text{Ni})_{87A} \times \frac{L_{12ec}}{L_{87A}} (M_{\odot}) \quad (1)$$

For the ^{56}Ni mass of SN 1987A we adopted the weighted mean of the values reported by Arnett & Fu (1989) and Bouchet et al. (1991), and for the bolometric luminosity we adopted the value of Bouchet et al. (1991) (see also Suntzeff et al. 1988). For SN 2012ec we calculated $M(^{56}\text{Ni})_{12ec} = 0.040 \pm 0.015 M_{\odot}$, which is an average of the estimates made at 138, 146 and 158 days (the reported uncertainty is the dispersion of the quoted values).

The evolution of the SED of SN 2012ec, based on optical and NIR photometry, is shown in Fig. 6. The observations covered the wavelength range 4000–23000 Å. We evaluated the SED evolution between 13 and 106 days and calculated blackbody continuum fits at each epoch. At +13 days the best fit gives a blackbody temperature around 9600 K, which decreases to 5300 K by day 126.

From the blackbody fit it was possible to evaluate the time evolution of the photospheric temperature of SN 2012ec. The temperature drops rapidly in the first 30 days from 9600 ± 800 K to 7000 ± 500 K, then it goes slowly down from 6500 ± 500 K to 5000 ± 400 K. The values of the temperature estimated by a fit on the photometric data differ from the one estimated by fitting the continuum in the spectra. The latter are higher at the early epochs when the spectra are dominated by the blue continuum and tend to be con-

sistent, within the errors, with the temperatures evaluated from the photometry starting from 50 days. In particular, in the first 30 days the spectroscopic temperature varies from 11900 ± 900 K to 8000 ± 700 K, decreasing to 6200 ± 500 at 50 days till reaching 5000 ± 500 K in the last epochs. The discrepancy between the two estimations of the temperature is due to the limited range of wavelength used for the fitting of the continuum from the spectra, compared with range used for the photometric fitting. When available the fit have been performed on a wavelength range of 4000–9000 Å, but sometimes only the range 4000–7000 Å was available for the fitting. We compared the estimated temperatures with the one of SN 2009bw (Inserra et al. 2012) and SN 1999em (Elmhamdi et al. 2003). SN 2012ec results to be redder at earlier phases since SN 2009bw has an initial temperature of ~ 12000 K and SN 1999em ~ 14300 K, while at late phases all converge to ~ 5000 K.

5 SPECTROSCOPIC EVOLUTION

5.1 Data sample and reduction

As a PESSTO follow-up target, SN 2012ec was scheduled for a dense spectroscopic monitoring campaign at the ESO NTT at La Silla, Chile. Ten epochs of optical spectra were acquired with the EFOSC2 and ten epochs of NIR spectra

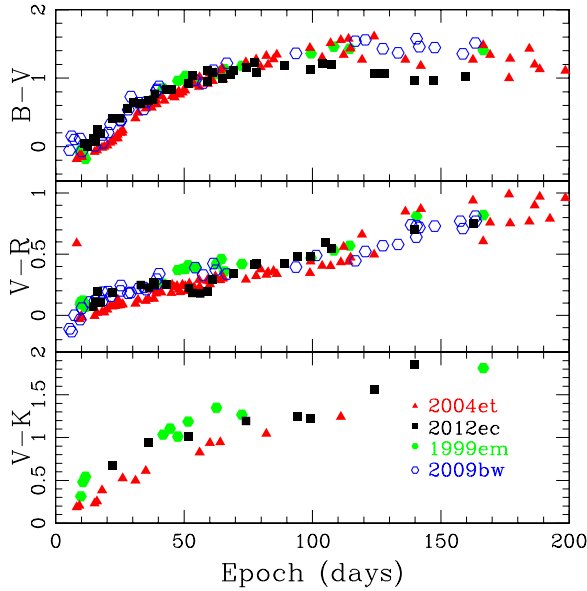


Figure 4. Colour evolution of SN 2012ec compared to those type IIP SNe.

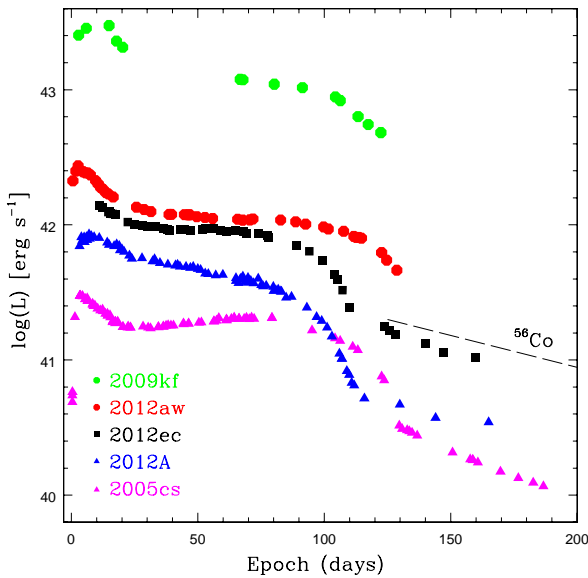


Figure 5. Pseudo-bolometric light curve of SN2012ec, along with those of other type IIP SNe. The pseudo-bolometric light curve accounts for the UBVRIJHK contributions for SN 2012A, UBgVr-RiIzJHK for SN 2012aw, griz for SN 2009kf and UBVRIJHK for SN 2005cs.

were gathered with SOFI. The optical dataset was supplemented with spectra from the following facilities: the 2.3m telescope of the Siding Spring Observatory (SSO, New South Wales, Australia) equipped with the Wide Field Spectrograph WiFeS (2 epochs), the 2.5m Nordic Optical Telescope (NOT, Canary Islands, Spain) equipped with the Andalusia Faint Object Spectrograph and Camera (ALFOSC) (1 epoch), the 1.82m Copernico Telescope (Asiago, Italy) equipped with AFOSC (3 epochs), the William Herschel

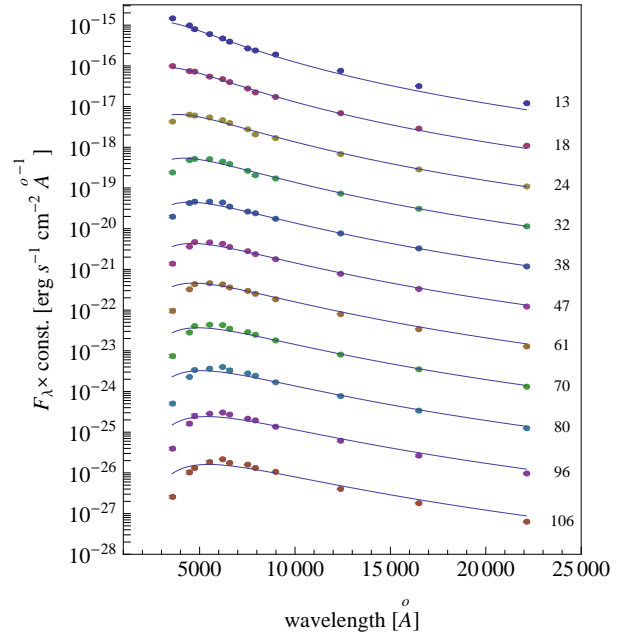


Figure 6. The temporal evolution of the SED of SN 2012ec. Circles represent the fluxes at the central wavelengths of each filter. Solid lines represent blackbody continuum fits. Fluxes are corrected for distance and extinction.

Telescope (WHT, Canary Islands, Spain) equipped with the Intermediate dispersion Spectrograph and Imaging system (ISIS) (1 epoch), the 1.22m Galileo Telescope (Asiago, Italy) equipped with the Boller & Chivens spectrograph (B&C) (2 epochs). The spectroscopic observations cover 29 epochs from day 8 to day 161. Details of the spectroscopic observations and the characteristics of the instrumentation utilised are listed in Table 7.

Spectra were pre-reduced (trimmed, overscan, bias and flat-field corrected) using the PESSTO pipeline (Smartt et al. 2014 *in preparation*), based on the standard IRAF tasks⁴. The wavelength calibration was performed using comparison spectra of arc lamps acquired with the same instrumental configuration as the SN observations. The science observations were flux calibrated with respect to observations of spectrophotometric standard stars. Further corrections for atmospheric extinction were applied using tabulated extinction coefficients for each telescope site (in the pipeline archive).

The quality of the flux calibration was checked by comparison of synthetic *BV* and *r* photometry derived from the spectra, using the IRAF task *CALCPHOT*, with the observed photometry at comparable epochs. These spectrophotometric magnitudes were compared to the ones obtained from photometric observations and, when necessary, a scaling factor was applied. Calibrated spectra were finally dereddened for the total line-of-sight extinction and then corrected for the heliocentric velocity of the host galaxy (see Table 1).

⁴ Fast reduction data are available on WISEREP (Yaron & Gal-Yam 2012) and full reduced data can be accessed from the ESO Phase 3 archive, all details on www.pessto.org

Table 7. Summary of instrumental sets-up used for the spectroscopic follow-up campaign.

Telescope	Instrument	Grism	Range [Å]	Resolution [Å]	# of epochs
NTT (3.58m)	EFOSC2	Gr11, Gr16	3350-10000	12	10
NTT (3.58m)	SOFI	GB	9400-14000	20	7
NTT (3.58m)	SOFI	GB, GR	14000-25000	20	3
CAO (1.82m)	AFOSC	Gr4	3500-8200	24	3
Pennar (1.22m)	B&C	Gr300	3400-7800	10	2
NOT (2.56m)	ALFOSC	Gr4	3400-9000	14	1
WHT (4.2m)	ISIS	R300B+R158R	3500-10000	5	1
ANU (2.3m)	WiFeS	B+R	3300-9000	2	2

NTT = New Technology Telescope with the optical camera ESO Faint Object Spectrograph and Camera EFOSC2 and with the Near-Infrared Camera Son of ISAAC (SOFI); CAO = the Copernico telescope at Asiago Observatory with the Asiago Faint Object Spectrograph and Camera (AFOSC); Pennar = Galileo telescope at Asiago Observatory with the Boller & Chivens spectrograph; NOT = Nordic Optical Telescope with the Andalucia Faint Object Spectrograph and Camera (ALFOSC); WHT = William Herschel Telescope with the Intermediate dispersion Spectrograph and Imaging System (ISIS); ANU = Australian National University telescope with the Wide-Field Spectrograph (WiFeS).

5.2 Data analysis

The time evolution of the optical spectrum of SN 2012ec, obtained from 8 to 161 days, is shown in Fig. 7 and corresponding line identifications are presented in Fig. 8.

Fig. 9 shows the evolution of the velocities of H_α , H_β , Fe II(5018 Å) and Fe II(5169 Å) for SN 2012ec. A list of line velocities is presented in Table 5.2.

Spectra at early phases show a blue continuum, broad Balmer lines and He I at 5876 Å. Lines show the typical P-Cygni profile, from which we estimate expansion velocities from the measurement of the position of the minimum of the absorption component. At early times, the estimated velocities are $12200 \pm 150 \text{ km s}^{-1}$ for H_α , $11000 \pm 150 \text{ km s}^{-1}$ for H_β and $10500 \pm 150 \text{ km s}^{-1}$ for He I. A blackbody fit to the continuum of these spectra, in the range 4000 – 9500 Å yielded a temperature $11900 \pm 900 \text{ K}$.

Spectra from day 21 to day 44 show in addition to the Balmer lines, some iron-group elements like Fe II (4629 Å), Fe II (5018 Å), Fe II (5169 Å) and Sc II (6246 Å). There is also a feature at 8200 Å due to the Ca II infrared triplet. The H_α velocity decreases to $10000 \pm 120 \text{ km s}^{-1}$, H_β to $9000 \pm 120 \text{ km s}^{-1}$, while the velocities for the Fe II(5018 Å) and Fe II(5169 Å) were measured to be $\sim 6000 \pm 100 \text{ km s}^{-1}$. At these epochs metal lines become prominent. The estimation of the temperature by a blackbody fit of the continuum drops from $8000 \pm 500 \text{ K}$ to $6000 \pm 300 \text{ K}$.

Spectra from day 49 to day 138 show the appearance of lines due to other heavy elements, such as Ba II(5981 Å), Ba II(6142 Å), Ti II(4100 Å), and numerous blends of Fe II lines, while the absorption feature of NaID is no longer visible due to the rise of these strong lines. At these phases the velocities decrease for all elements, H_α reaches to $5000 \pm 90 \text{ km s}^{-1}$, Fe II (5018 Å) and Fe II (5169 Å) to $2000 \pm 120 \text{ km s}^{-1}$. The presence of the iron-group line blends prevents the detection of H_β . A fit to the continuum yields a temperature of $5000 \pm 400 \text{ K}$.

At late times, the spectrum at 161 days shows forbidden [O I] lines (6300, 6364 Å) and the semi-forbidden Ca II] doublet (7291, 7394 Å).

The ejecta velocities of SN 2012ec have been compared with those measured for other Type IIP SNe: SN 2012A, SN

2012aw, SN 2004et and SN 1999em (see Table 8). At early phases, the H_α velocity is lower than that estimated for SN 2012aw ($\sim 14000 \text{ km s}^{-1}$; Dall’Ora et al. 2014), but higher than the one estimated for SN 2012A ($\sim 10200 \text{ km s}^{-1}$) (Tomasella et al. 2013), and comparable with the one of SN 1999em ($\sim 12000 \text{ km s}^{-1}$) (Elmhadi et al. 2003). At later phases (40 days), the Fe II (5169 Å) velocities are higher than those estimated for SN 2012A ($\sim 3500 \text{ km s}^{-1}$), comparable with those of SN 2004et ($\sim 4000 \text{ km s}^{-1}$) and SN 1999em ($\sim 4200 \text{ km s}^{-1}$). But they are still lower than that of SN 2012aw ($\sim 5500 \text{ km s}^{-1}$). This trend is confirmed at late stages. In summary, the ejecta velocities measured for SN 2012ec velocities are similar to those measured for SNe 1999em and 2004et, but are consistently lower than for SN 2012aw and higher than for SN 2012A.

A close-up with the time evolution of the H_α , H_β and Ca II lines profile in SN 2012ec is shown in Fig. 10.

The NIR spectra cover the period from day 21 to day 161 (Fig. 11). The H I Paschen lines are clearly visible at all epochs. Starting from day 68 we identify also He I and Ca I lines and Br_γ . The elements identified in the NIR spectra (Fig. 8) are typical of Type IIP SNe, in particular the spectra at 71 and 79 days are similar to the NIR spectrum of SN 2012A at 72 days (Tomasella et al. 2013).

6 HYDRODYNAMIC MODELING

To constrain the main physical properties of the progenitor and the energetics of the explosion, we performed hydrodynamical modelling of SN 2012ec. Among the most important parameters we needed to constrain the ejected mass, the radius of the progenitor, the explosion energy and the ejected ^{56}Ni mass (Zampieri et al. 2003; Kasen & Woosley 2009). These were found by comparing the observed bolometric luminosity, the evolution of line velocities and continuum temperature at the photosphere with the corresponding simulated quantities (Zampieri et al. 2003; Pumo et al. 2010). The comparison procedure consists of performing a simultaneous χ^2 fit of all the relevant observables against those predicted by the model calculations, and was successfully adopted for other CC-SNe (e.g. SN 2007od,

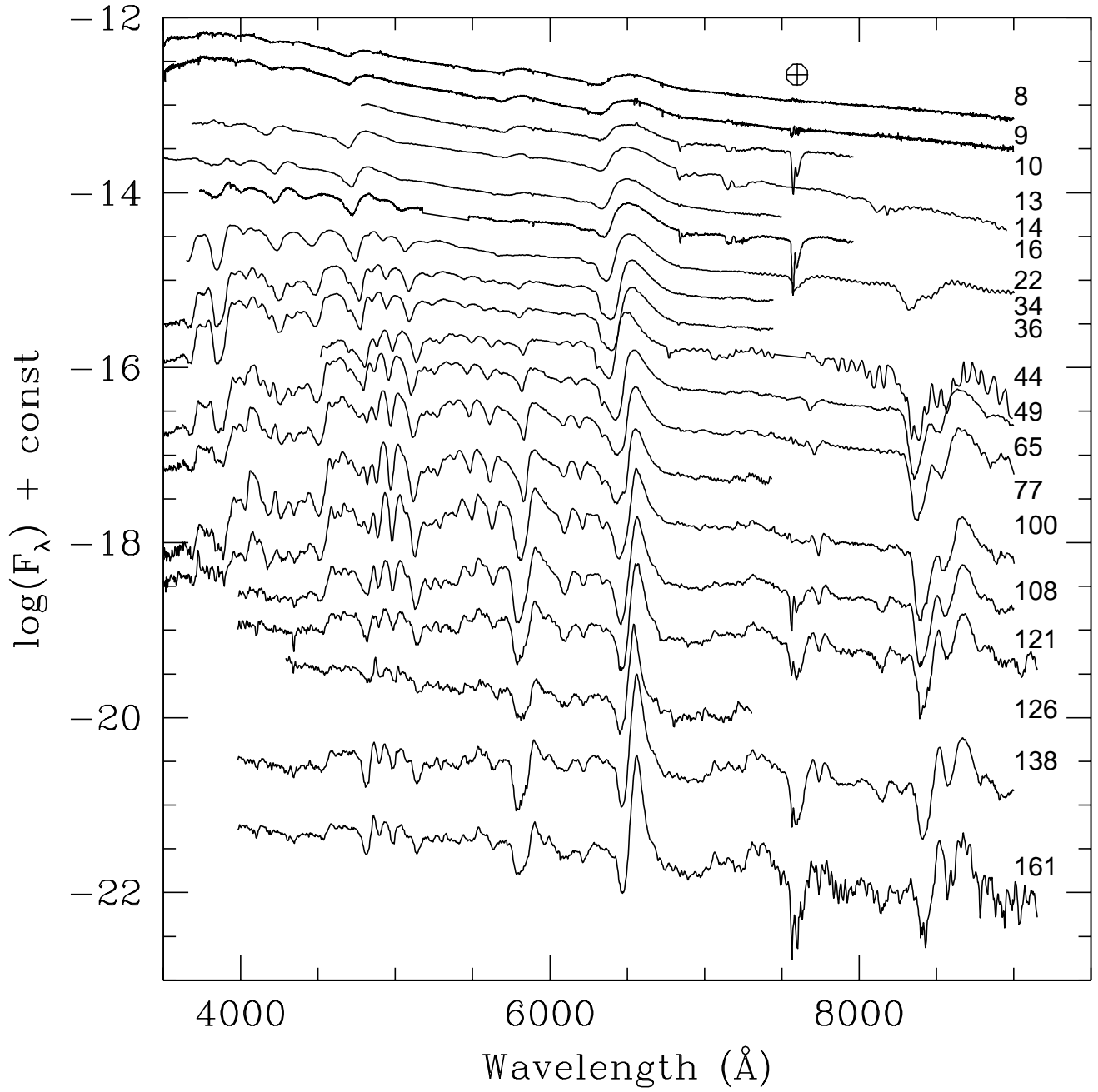


Figure 7. Optical spectroscopic evolution of SN2012ec during the photospheric phase, starting from +8, from the explosion epoch, to +161 days.

Table 8. Expansion velocity of SN 2012ec at selected epochs, compared to other Type IIP SNe.

	2012aw	2012ec	1999em	2004et	2012A
H_{α} (~ 10 d)	14000	12200	12000		10200
Fe II (~ 40 d)	5500	4100	4200	4000	3500
Fe II (~ 100 d)	3000	2400	2000	2000	2000

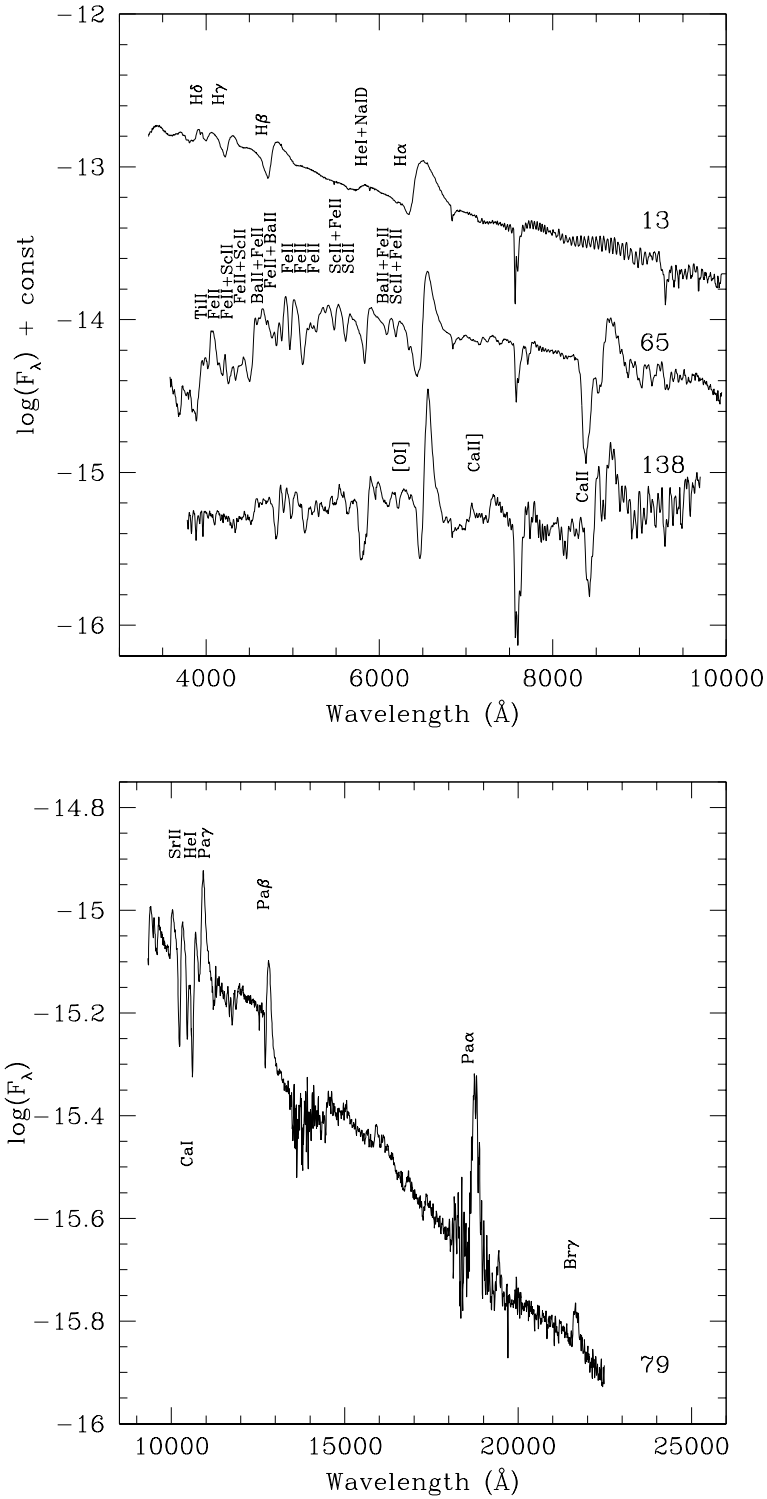


Figure 8. Identifications of line features observed in optical (at three characteristic epochs; top panel) and NIR spectra (bottom panel) of SN 2012ec.

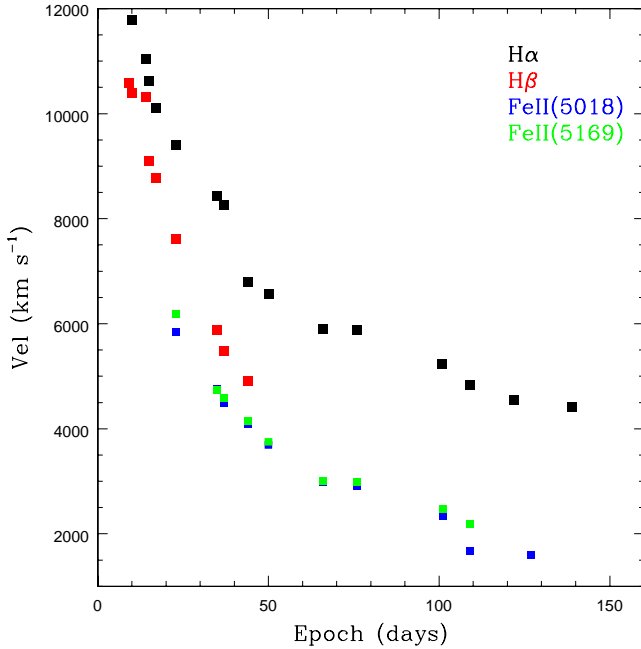
Inserra et al. 2011; SN 2009bw, Inserra et al. 2012; SN 2009E, Pastorello et al. 2012; SN 2012A, Tomasella et al. 2013 and SN 2012aw, Dall’Ora et al. 2014).

The hydrodynamical modelling of the explosion was performed with two different codes: a semi-analytic code

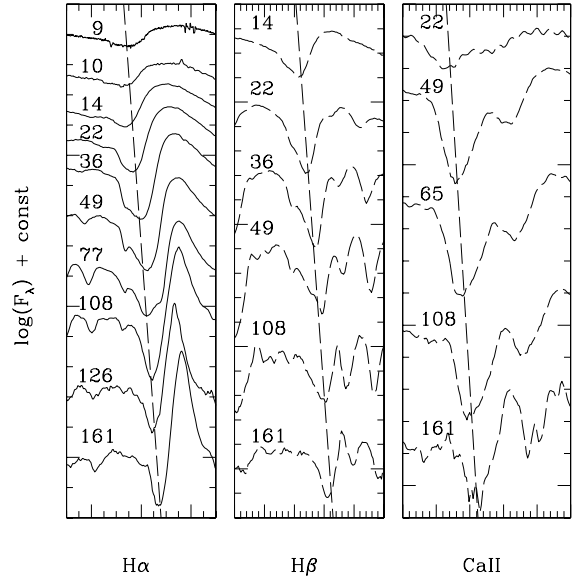
(Zampieri et al. 2003), that solves the energy balance equation for a constant density envelope which expands homologously; and a radiation-hydrodynamics code (Pumo & Zampieri 2011), that can simulate the full radiative-hydrodynamical evolution of the ejected material.

Table 9. Measured expansion velocities (from the minima of P-Cygni absorption) for SN 2012ec. Estimated uncertainties are in parentheses

Date	MJD	Epoch ^a (d)	$H\alpha$ km s^{-1}	$H\beta$ km s^{-1}	$FeII(5018)$ km s^{-1}	$FeII(5169)$ km s^{-1}	$ScII(5533)$ km s^{-1}	$CaII(8520)$ km s^{-1}
20120812	56152	8	12200 (150)	10600 (150)				
20120813	56153	9	11800 (130)	10400 (150)				
20120817	56157	13	11000 (160)	10300 (130)				
20120818	56158	14	10600 (120)	9100 (120)				
20120820	56160	16	10100 (120)	8800 (110)				
20120826	56166	22	9400 (100)	7600 (120)	5800 (100)	6200 (100)		
20120907	56178	34	8400 (110)	5900 (110)	4700 (100)	4700 (120)	5000 (120)	
20120909	56180	36	8300 (110)	5500 (130)	4500 (110)	4600 (100)	4600 (130)	
20120916	56187	43	6800 (120)	4900 (110)	4100 (110)	4100 (130)		
20120922	56193	49	6600 (110)		3700 (100)	3700 (100)	3800 (140)	5600 (120)
20121008	56209	56	5900 (110)		3000 (100)	3000 (140)	3100 (100)	4900 (140)
20121017	56219	75	5800 (170)		2900 (110)	2900 (150)		
20121112	56244	100	5230 (120)		2300 (120)	2400 (100)	2100 (130)	4100 (100)
20121122	56252	108	4800 (100)			2200 (100)	2000 (150)	3700 (150)
20121203	56265	121	4500 (100)		2000 (110)			3600 (130)
20121212	56270	126			1600 (100)			
20121220	56282	138	4400 (100)					3500 (140)

^a = epoch from the explosion.**Figure 9.** Ejecta velocity evolution, estimated from the $H\alpha$, $H\beta$, $Fe II(5018 \text{ \AA})$ and $Fe II(5169 \text{ \AA})$ lines.

The latter code solves the hydrodynamic equations of a self-gravitating, relativistic fluid interacting with radiation, and incorporates an accurate treatment of radiative transfer and of the evolution of the ejected material, considering both the gravitational effect of the compact remnant and the heating effects related to the decays of radioactive isotopes synthesized during the CC SN explosion. The first code is used to investigate the more likely parameter space and provide a robust, first estimate of the best fitting model. A more detailed and time-consuming search is then performed with the radiation-hydrodynamics code. This modeling is appropriate only if the emission from the CC SN is dominated by freely expanding ejecta. Clearly, interaction with the circum-

**Figure 10.** Time evolution of $H\alpha$, $H\beta$ and $Ca II$ NIR triplet for SN 2012ec.

stellar medium (CSM) can affect the early evolution of the light curve in a way not presently predicted by the model.

An extended grid of semi-analytic models was computed, covering a wide range in mass. The χ^2 distribution of the models as a function of ejected mass is shown in Fig. 12 and shows two comparable minima, one at $\sim 9.1 M_\odot$, the other at $\sim 12.6 M_\odot$. The best fit model corresponding to the first minimum ($9.1 \pm 0.8 M_\odot$) has an initial radius of $\sim 2.3 \times 10^{13} \pm 0.7 \text{ cm}$ ($330 \pm 100 R_\odot$), a total explosion energy of $\sim 0.7 \pm 0.2 \text{ foe}$ and an ejected ^{56}Ni mass of $\sim 0.035 M_\odot$. The best fit model corresponding to the second minimum has an initial radius of $1.6 \pm 0.5 \times 10^{13} \text{ cm}$ ($230 \pm 70 R_\odot$), a total explosion energy of $1.2 \pm 0.4 \text{ foe}$, and an ejected ^{56}Ni mass of $\sim 0.035 M_\odot$. In light of the results of the progenitor detection, in the following we consider only the “high-mass” minimum. The best fit model corresponding to the second

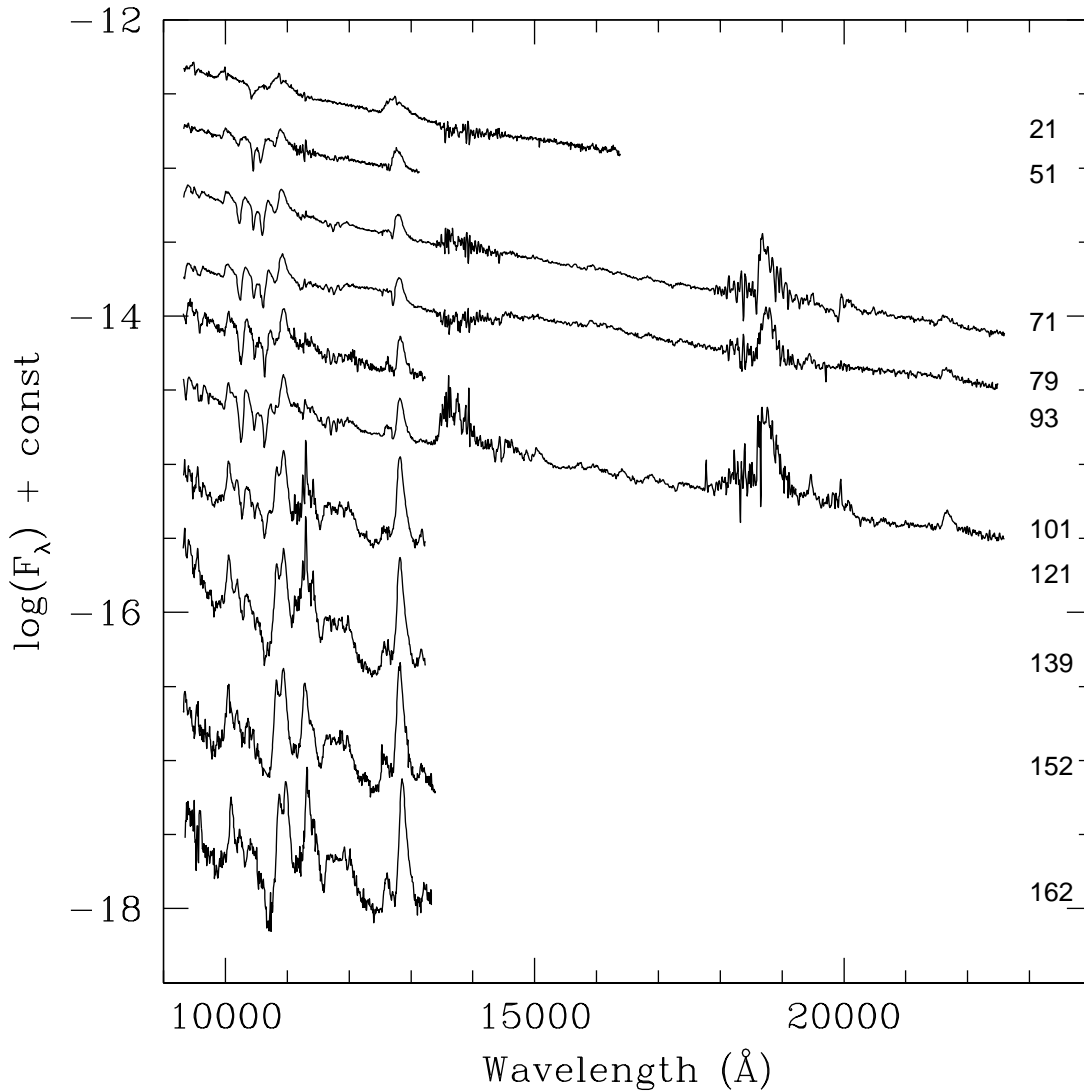


Figure 11. NIR spectroscopic evolution of SN 2012ec. Individual spectra have been shifted in flux for clarity. Numbers on the right indicate the epochs from explosion.

minimum is shown in Fig. 13 and appears to be in good agreement with all the observables.

7 COMPARISON WITH WELL STUDIED SNE IIP

In this section, we present a detailed comparison of SN 2012ec with two well studied Type IIP SNe: 2012A and 2012aw. In all three cases, a progenitor was detected in pre-explosion images and sufficient photometric and spectroscopic observations were available to permit a homogenous analysis of the properties of the SNe using hydrodynamical models. SN 2012ec was discovered 9 days after the explosion, while the other SNe were discovered much sooner after explosion, see Table 10. SN 2012aw was discovered in M95 at a distance modulus $\mu = 29.96 \pm 0.04$ mag and with a total reddening of $E(B - V) = 0.086$ mag; SN 2012A was discov-

ered in NGC 3239 at $\mu = 29.96 \pm 0.15$ and $E(B - V) = 0.037$ mag.

The estimates of the initial masses of the progenitors, through direct detection of the precursor, were: $M_{12aw} = 14 - 26 M_{\odot}$ (Fraser et al. 2012), M_{12ec} in the range $14 - 22 M_{\odot}$ (Maund et al. 2013) and $M_{12A} = 8 - 15 M_{\odot}$ (Tomasella et al. 2013). In a separate analysis of the pre-explosion observations of SN 2012aw Van Dyk et al. 2012 reported an initial mass of $15 - 20 M_{\odot}$. A major uncertainty in estimating the progenitor mass is degeneracy between temperature and reddening. Kochanek et al. 2012 showed that a different treatment of the extinction results in a luminosity of $\log(L/L_{\odot}) = 4.8 - 5.0$, corresponding to a progenitor main sequence mass of $13 - 16 M_{\odot}$ (Jerkstrand et al. 2014), which is in agreement with the nebular spectral modelling and the amount of oxygen produced by SN 2012aw.

Fig. 14 shows the photometric evolution of the absolute magnitudes in the R and V bands of SN 2012ec, SN

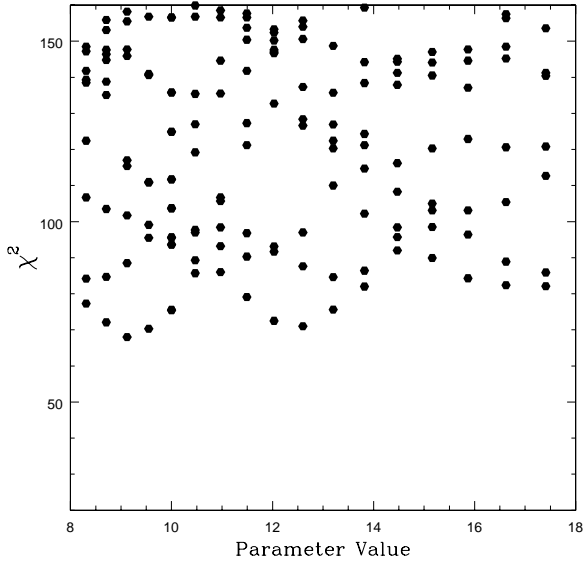


Figure 12. χ^2 distribution of the fit of the semi-analytical model to the observed quantities, as a function of the estimated ejected mass.

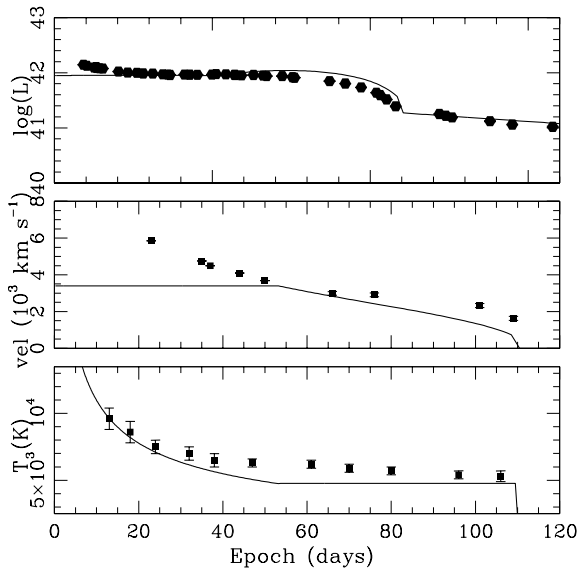


Figure 13. Time evolution of the main observables of SN 2012ec (filled dots), compared to the “high-mass” best fit model (solid line). The top panel shows the fit of the bolometric light curve; the middle panel shows the fit of the Fe II velocity and the bottom panel shows the fit of the continuum temperature.

2012aw and SN 2012A. We note that SN 2012ec is intermediate between the more luminous SN 2012aw and the fainter SN 2012A. The duration of the plateau and the post-plateau decline is longer in SN 2012aw and shorter and steeper in SN 2012A. Again, SN 2012ec shows an intermediate behaviour, with quite a short plateau and a slower post-plateau drop. The absolute magnitude in the R band for these SNe, on the plateau (~ 60 days), were $M_R(12aw) = -17.1$ mag, $M_R(12ec) = -16.7$ mag and $M_R(12A) = -16.2$ mag.

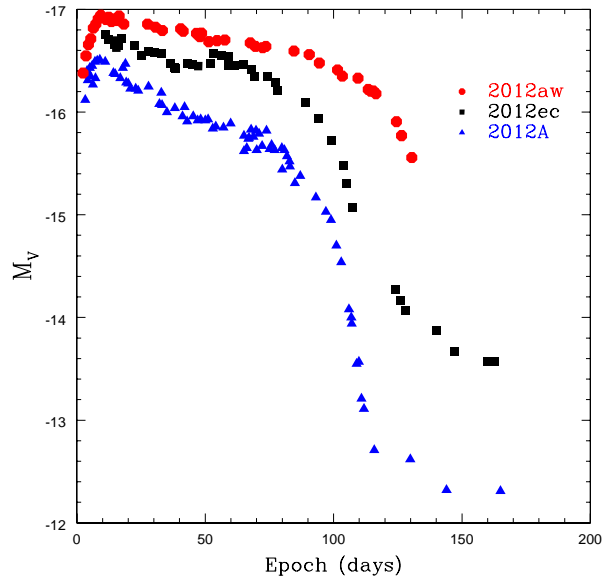
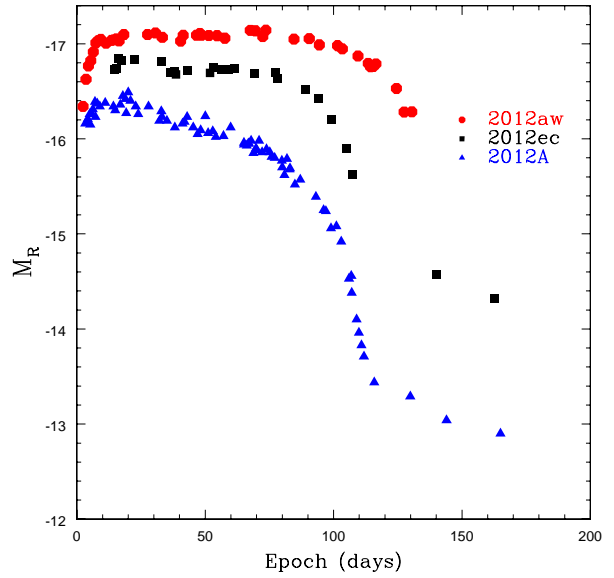


Figure 14. Comparison of the light curves in the R (top panel) and V (bottom panel) bands of SN 2012ec, with SN 2012aw and SN 2012A.

A comparison of the colours evolution of SN 2012ec with SN 2012aw and SN 2012A is shown in Fig. 15. The colour of each SN has been corrected for reddening for a proper comparison. The colour evolution of SN 2012ec has already been discussed in Sect. 4.2. We can see that the colour evolution of SN 2012ec is similar to that of the other two SNe.

Fig. 16 shows a comparison of the bolometric light curves of SNe 2012ec, 2012A and 2012aw, where SN 2012ec is of intermediate luminosity between the other two SNe. In particular, during the plateau phase, SN 2012ec is more luminous than SN 2012A and exhibits a longer plateau. Conversely, SN 2012aw is clearly of higher luminosity than SN 2012ec throughout the entirety of the photospheric phase and has a longer plateau 100 days (Dall’Ora et al. 2014).

From the comparison of the ^{56}Ni mass estimated for

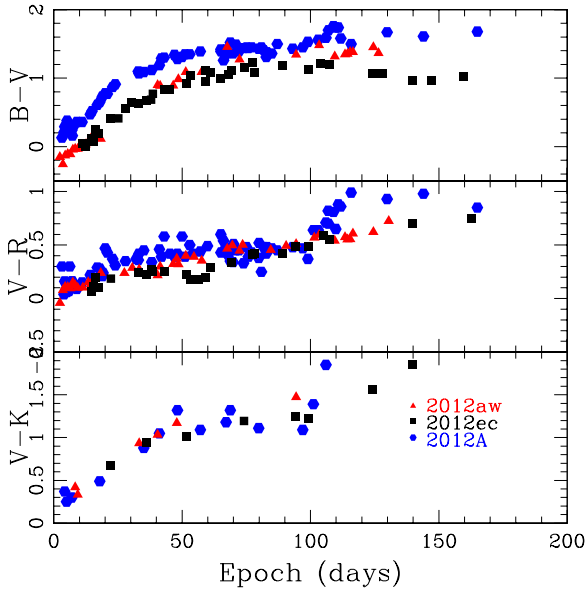


Figure 15. Comparison of the colour evolution of SN 2012ec, in the $B-V$ (top panel), $V-R$ (middle panel), and $V-K$ (bottom panel), with SN 2012aw and SN 2012A.

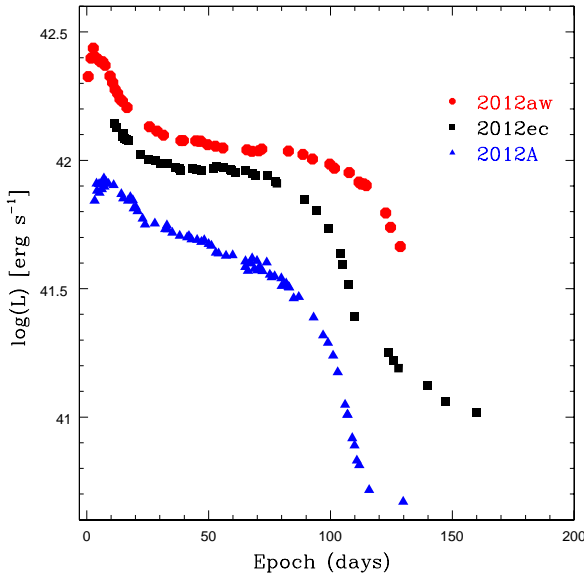


Figure 16. Pseudo-bolometric light curve of SN 2012ec, compared to SN 2012aw and SN 2012A.

the three SNe we find out it to be comparable within the errors may note a sequence in the values: $M(^{56}\text{Ni})_{12aw} = 0.056 \pm 0.013 M_{\odot}$, $M(^{56}\text{Ni})_{12ec} = 0.040 \pm 0.015 M_{\odot}$ and $M(^{56}\text{Ni})_{12A} = 0.011 \pm 0.004 M_{\odot}$.

In Fig. 17 we show a comparison of the spectra of SN 2012ec with those of SN 2012aw and SN 2012A at three different epochs, highlighting the spectroscopic similarities between the three SNe at all epochs.

We also compared the SN 2012ec ejecta velocities measured from H_{α} , and Fe II(5169 Å) with the velocities estimated for other type IIP SNe (see Fig. 18). SN 2012aw

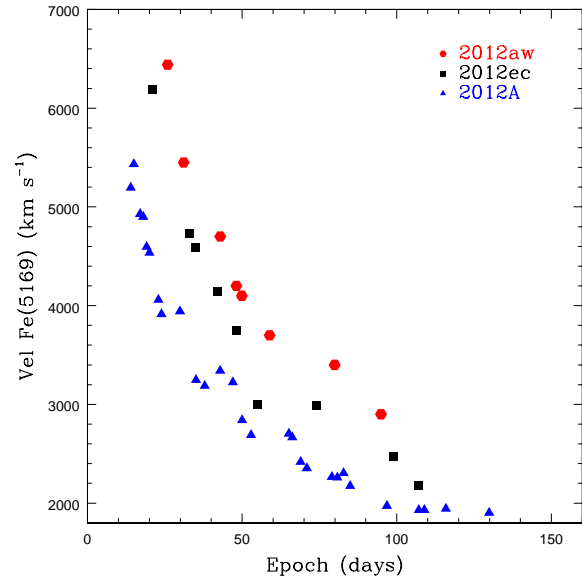
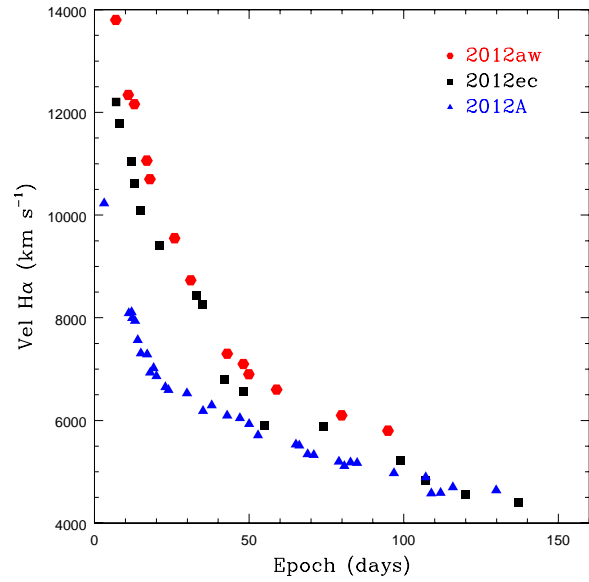


Figure 18. Comparison of the ejecta velocities of SN 2012ec, SN 2012A and SN 2012aw, from the H_{α} (top panel) and from the Fe II(5169 Å) lines (bottom panel).

has an initial H_{α} velocity $\sim 14000 \text{ km s}^{-1}$, higher than those of SN 2012ec ($\sim 12200 \text{ km s}^{-1}$) and of SN 2012A ($\sim 10200 \text{ km s}^{-1}$). After 100 days, the H_{α} decrease to $\sim 6000 \text{ km s}^{-1}$ for SN 2012aw, still being higher of those of SN 2012ec ($\sim 5000 \text{ km s}^{-1}$) and of SN 2012A ($\sim 5000 \text{ km s}^{-1}$). The initial Fe II(5169 Å) of SN 2012aw is $\sim 6500 \text{ km s}^{-1}$, still higher than those of SN 2012ec ($\sim 6000 \text{ km s}^{-1}$) and of SN 2012A ($\sim 5200 \text{ km s}^{-1}$). After ~ 100 days it drops to $\sim 3000 \text{ km s}^{-1}$ for SN 2012aw, to $\sim 2500 \text{ km s}^{-1}$ for SN 2012ec and to $\sim 2000 \text{ km s}^{-1}$ for SN 2012A. In terms of ejecta velocities, SN 2012ec is intermediate between SN 2012aw and SN 2012A.

A comparison of the temperature estimated via black-body fitting of the SED evolution for the 3 SNe is presented in Fig. 19, from which it is clear that the temperature evo-

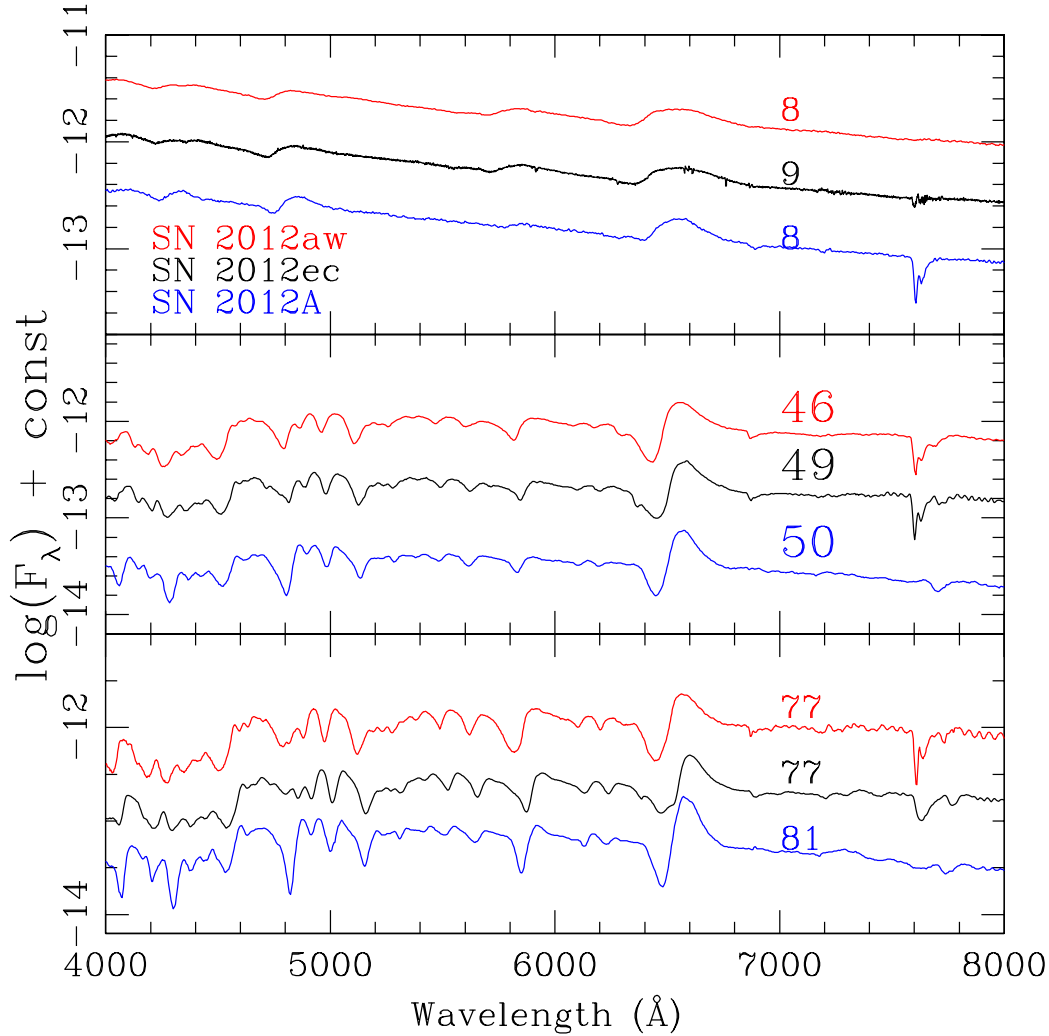


Figure 17. Comparison of the spectra of SN 2012ec, SN 2012aw and SN 2012A at three different epochs, i.e. at early stage, during the plateau phase and at the end of the plateau.

lutions of SN 2012ec and SN 2012A are similar, and significantly hotter than SN 2012aw (from $\sim 20 - 30$ days post-explosion).

The ejected mass calculated for SN 2012ec is $12.6 M_{\odot}$, which is comparable to the value estimated for SN 2012A ($12.5 M_{\odot}$ Tomasella et al. 2013), but lower than value calculated for SN 2012aw ($20 M_{\odot}$, Dall’Ora et al. 2014). Similarly the initial radius for SN 2012ec is comparable to SN 2012A ($\sim 260 R_{\odot}$), but smaller than for SN 2012aw ($\sim 400 R_{\odot}$). Conversely, the estimated energy of SN 2012ec of $1.2 foe$ is higher than the value estimated for SN 2012A ($0.48 foe$) but similar to the energy of SN 2012aw ($1.5 foe$).

In summary, SN 2012ec is more luminous than SN 2012A, synthesized more ^{56}Ni and has higher expansion velocities. The ejecta masses of the two SNe are comparable, but the pre-SN radius and the masses of the progenitors are slightly different. This indicates that the progenitor of SN 2012ec progenitor was likely to be more massive, but more compact the progenitor of SN 2012A. SN 2012aw has a larger initial radius, a more massive envelope and more energetic explosion that produced more ^{56}Ni and higher ejecta

velocities than SN 2012ec. The main characteristics of this comparison are summarised in Table 10.

8 TYPE IIP SNE AS STANDARD CANDLES

The extragalactic distance scale is intimately connected with Type Ia SNe, up to cosmological distances, and through Type Ia SNe the acceleration of the Universe was discovered (Perlmutter et al. 1999; Riess et al. 1998; Schmidt et al. 1998). At the present time, current facilities allow us to detect and study Type Ia SNe up to $z = 1.7$ (Rubin et al. 2013), while the next generation of extremely large telescopes will allow us to study Type Ia SNe up to $z \sim 4$ (Hooke 2013). At high z , however, the number of Type Ia SNe may significantly decrease, due to the long lifetimes of their progenitors. Alternatively, the ubiquitous Type II (core-collapse) SNe could be an appealing choice to probe further cosmological distances. While Type Ia SNe are the product of an old to intermediate stellar population, Type II SNe come essentially from a young stellar population, and

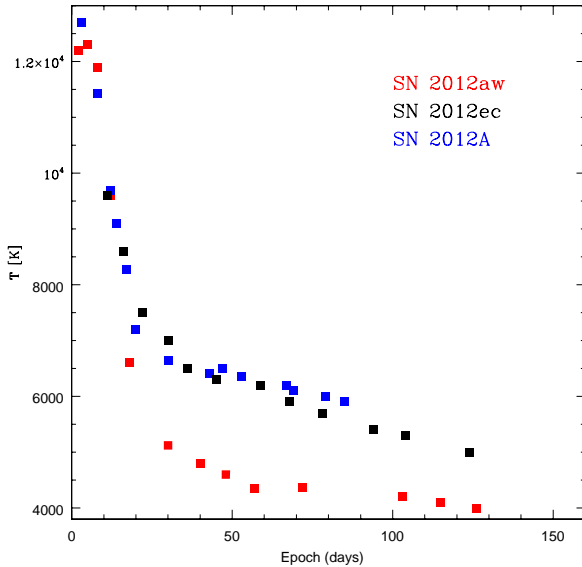


Figure 19. Comparison of the time evolution of the photospheric temperature of SN 2012ec, with SNe 2012A and 2012aw.

Table 10. Comparison of the main parameters of SN 2012ec, SN 2012aw and SN 2012A.

	SN 2012aw	SN 2012ec	SN 2012A
μ (mag)	29.96	31.19	29.96
E(B-V) (mag)	0.086	0.124	0.037
MJD_{expl} (d)	56002	56151	55933
MJD_{disc} (d)	56003	56143	55934
v_{FeII} ($km\ s^{-1}$) ^a	~ 4200	~ 3700	~ 2800
M_R (mag)	-17.1	-16.7	-16.2
$L(10^{42} erg\ s^{-1})$ ^b	1.1	0.9	0.5
^{56}Ni (M_{\odot})	0.056	0.040	0.011
E (foe) ^c	1.5	1.2	0.48
R (10^{13} cm)	3	1.6	1.8
M_{eject} (M_{\odot})	20	12.6	12.5
M_{prog} (M_{\odot}) ^d	13-16	14-22	8-15

^a at ~ 50 days

^b at the plateau

^c 1 foe = 10^{51} erg

^d Mass of the progenitor as estimated from the pre-explosion images

thus constitute a homogeneous sample with respect to the age of the stellar population. It should also be noted, however, that type II SNe are significantly fainter than Type Ia SNe and that they explode in younger and dustier regions, making their discovery and study more difficult.

Although the characteristics of the light curves of the Type II SNe (peak luminosity, decline rate, presence and duration of the plateau) span a broad range of values, their use as distance indicators was already recognized by Kirshner & Kwan (1974), who applied the Baade-Wessellink analysis to SN 1969L and SN 1970G through the Expanding Photosphere Method (EPM), and by Mitchell et al. (2002) who modified the EPM method by introducing the spectral synthesis analysis (Spectral-fitting Expanding Atmosphere

Method, SEAM). Both EPM and SEAM were successfully applied during the years up to cosmological distances (e.g. Baron et al. 2004, Schmidt et al. 1994), but to be properly applied they require a good sampling of the light curves and high quality spectra.

More specifically, for type IIP SNe Hamuy & Pinto (2002) found a tight empirical correlation between the bolometric luminosity and the expansion velocity of the ejecta during the plateau phase. The luminosity and the expansion velocity (as measured from the Fe II (5169) line) are estimated at approximately the “half plateau” phase, conventionally set at 50 days. This method, dubbed the “Standardized Candle Method” (SCM), was subsequently investigated by Nugent et al. (2006), Poznanski et al. (2009), D’Andrea et al. (2010) and by Olivares et al. (2010), with the advantage that it requires less input data than EPM and SEAM. The empirical correlation at the base of the SCM was theoretically reproduced by Kasen & Woosley (2009), who pointed out that the correlation relies on the simple behaviour of the expanding hydrogen envelope. However, they also warned that SCM may be sensitive to the progenitor metallicity and mass, that in turn could lead to systematic effects.

Almost all the quoted calibrations adopt 50 days post-explosion as a reference phase that roughly corresponds to the “half-plateau”. Other choices for the reference phase during the plateau phase can be set, but with the *caveat* that the velocity measured from the Fe II (5169) line is moderately decreasing over the duration of the plateau and that the method requires knowledge of the epoch of the explosion. Only Olivares et al. (2010) adopted a “custom” reference phase for each SN, due to the fact that the length of the plateau varies from SN to SN. For this reason, they suggested adopting a reference epoch 30 days prior to epoch at which the light curve has declined to a brightness midway between the plateau brightness and the brightness at which it joins the radioactive tail.

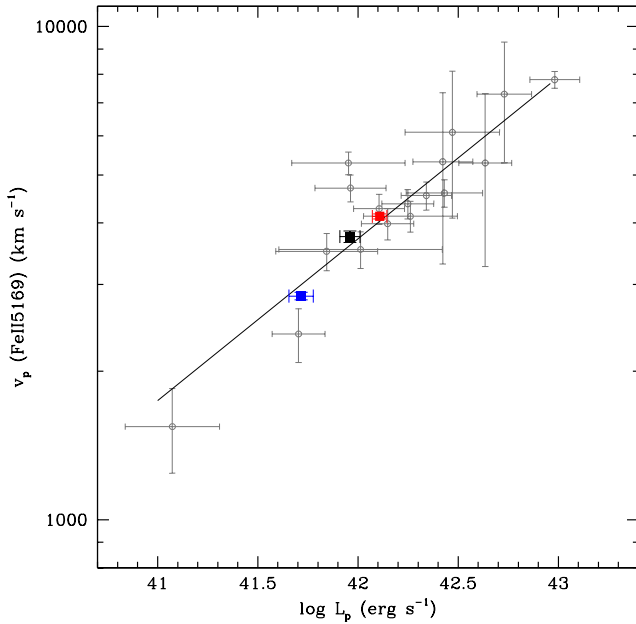
In this paper we take advantage of the homogeneous analysis of the three type IIP SNe, SN 2012ec, SN 2012aw and SN 2012A, to perform a detailed comparison of the available calibrations of SCM and assess the robustness of the method. More specifically, for the comparison we adopt the *I*-band calibrations of SCM, namely: eq. 2 of Hamuy & Pinto (2002); eq.1 of Nugent et al. (2006); eq. 2 of Poznanski et al. (2009); eq. 2 of D’Andrea et al. (2010); and eq. 16 of Olivares et al. (2010). Our estimated distances to the three SNe are compared with a homogeneous set of distances, based on primary (Cepheids, Tip of the Red Giant Branch, or TRGB) and secondary distance indicators (Tully-Fisher, Surface Brightness Fluctuations or SBF), available in the Extragalactic Distance Database (Tully et al. 2009). In Table 11 we report, for each SN, the distance estimated with the above calibrations. Moreover, we show the difference between the SCM distance and the estimates from the primary (when available) and secondary distance indicators. Finally, for each calibration, we report the mean difference and dispersion of the SCM distances with the estimates based on the primary and secondary distance indicators.

Table 11 may suggest that the Hamuy & Pinto (2002) calibration gives more homogenous results with respect to other calibrations. However, it must be noted that our test is based on only three SNe and that all the calibrations are con-

Table 11. Comparison of the SCM distances and the estimates from the primary and secondary distance indicators.

Calibration	SN	SCM (mag)	Primary (mag)	Secondary (mag)	SCM – Primary (mag)	SCM - Secondary (mag)	Mean residual (mag)
HP2002	SN 2012ec	31.22 ± 0.3		31.19		0.03	
	SN 2012aw	29.96 ± 0.3	29.96	30.00	0.00	−0.04	0.01 ± 0.04
	SN 2012A	30.05 ± 0.3		30.00		0.05	
Nugent06	SN 2012ec	31.29 ± 0.3		31.19		0.10	
	SN 2012aw	30.03 ± 0.3	29.96	30.00	0.07	0.03	0.13 ± 0.09
	SN 2012A	29.77 ± 0.3		30.00		−0.23	
Poznanski09	SN 2012ec	31.15 ± 0.2		31.19		−0.04	
	SN 2012aw	29.70 ± 0.2	29.96	30.00	−0.26	−0.30	$−0.1 \pm 0.14$
	SN 2012A	30.04 ± 0.2		30.00		0.04	
Olivares10	SN 2012ec	31.11 ± 0.2		31.19		−0.08	
	SN 2012aw	29.58 ± 0.2	29.96	30.00	−0.38	−0.42	$−0.01 \pm 0.37$
	SN 2012A	30.47 ± 0.2		30.00		0.47	
D’Andrea10	SN 2012ec	31.33 ± 0.2		31.19		0.14	
	SN 2012aw	29.86 ± 0.2	29.96	30.00	−0.10	−0.14	0.09 ± 0.17
	SN 2012A	30.27 ± 0.2		30.00		0.27	

Quoted errors for the SCM distances are the standard deviations of the individual calibrations. The value of the distance from the primary indicators of SN 2012aw is the average from the Cepheids (Freedman et al. 2001) and the TRGB (Rizzi et al. 2007) estimates. Finally, the “mean residual” column shows the average of the SCM – Secondary values, where the error is the standard deviation.

**Figure 20.** Our studied sample of type IIP SNe: SN 2012ec (black), SN 2012aw (red) and SN 2012A (blue) in the original Hamuy & Pinto (2002) plane.

sistent within the errors. We note that the Hamuy & Pinto (2002) calibration was derived assuming a value of $H_0 = 65 \text{ km s}^{-1} \text{ Mpc}^{-1}$, significantly lower than the estimate of $H_0 = 73.8 \pm 2.4 \text{ km s}^{-1} \text{ Mpc}^{-1}$ of Riess et al. (2011), but in agreement with $H_0 = 63.7 \pm 2.3 \text{ km s}^{-1} \text{ Mpc}^{-1}$ given by Tammann & Reindl (2013). The large scatter in the Olivares et al. (2010) calibration could be due to the difficulty in estimating the reference phase, when a good sam-

pling of the light curve, during the fall from the plateau, is not available. All these calibrations rely on moderately distant SNe, embedded in the Hubble flow or for which SBF distances are available. However, these distances could still be affected by systematics not completely understood. For these reasons a new calibration of the SCM, based on nearby type IIP SNe for which primary (Cepheids and TRGB) and homogenous secondary indicators (TRGB) distances are available, would be of great interest. Moreover, for these SNe the metallicity effects suggested by Kasen & Woosley (2009) could also be investigated. The average of the five individual estimates of the distances of SN 2012ec gives $31.22 \pm 0.08 \text{ mag}$, that we adopt as our final SCM-based distance. This value is in excellent agreement with the Tully-Fisher distance of 31.19 ± 0.13 , adopted for our analysis.

9 CONCLUSIONS

We have presented the results of the Large Program “Supernova Variety and Nucleosynthesis Yields” and PESSTO photometric and spectroscopic monitoring campaign of SN 2012ec. This is one of the most intensively observed and well investigated Type IIP SNe to date. The optical and spectroscopic monitoring during the photospheric phase lasted for ~ 161 days and allowed us to determine the evolution of the pseudo-bolometric luminosity, the expansion velocity and the photospheric temperature and ^{56}Ni mass. These parameters, used in a hydrodynamical model, allowed us to estimate the explosion parameters such as the explosion energy, the envelope mass and the pre-SN radius. Correcting the data for reddening ($E(B - V) = 0.14 \pm {}^{+0.15}_{-0.12} \text{ mag}$) and distance modulus ($\mu = 31.19 \pm 0.13$) we estimated the luminosity to be $L = 0.9 \times 10^{42} \text{ erg s}^{-1}$, at the plateau and evaluated the ^{56}Ni mass to be $0.040 \pm 0.015 M_{\odot}$. The spectra of SN 2012ec were dominated by Balmer lines in the early

epochs and after 20 days the iron-group elements start to appear and become more prominent with time. The NIR spectra were dominated by Paschen lines and, starting from 68 days, it is possible to identify the He I, Ca I and the Brackett Br_γ . A black body fit to the continuum gives temperature of 11900 ± 900 K in the early epochs decreasing to 6200 ± 500 K at 50 days and 5000 ± 500 K in the last epochs. From the spectroscopic dataset we estimate an initial velocity of 12200 km s^{-1} for the H_α line and 11000 km s^{-1} for H_β . The H_α velocity decreases to 5000 km s^{-1} at 50 days. At ~ 25 days the iron-group elements appear, for which we measure a velocity of 6000 km s^{-1} for the Fe II. The behaviour of SN 2012ec is similar to that seen in other IIP SNe, such as SN 1999em (Elmhamdi et al. 2003) and SN 2004et (Maguire et al. 2010). We estimate the physical parameters of SN 2012ec through the hydrodynamical modeling described in Sect. 6. The fit suggests an ejected mass of $M_{env} = 12.6 M_\odot$, a pre-SN radius of $R = 1.6 \times 10^{13} \text{ cm}$, an explosion energy of $E = 1.2 \text{ foe}$ and an ejected $M(^{56}\text{Ni}) = 0.035 M_\odot$. The progenitor mass is in agreement with independent estimate of Maund et al. (2013) $M = 14 - 22 M_\odot$ obtained by analyzing pre-explosion images. Previously reported ejecta masses estimated from hydrodynamical modelling are generally too large compared to the initial mass estimated from direct detections of the progenitor on pre-explosion images (Utrobin & Chugai 2008; Maguire et al. 2010). In order to investigate this discrepancy, we performed an homogeneous comparison between three type IIP SNe, estimating the mass of the progenitor with two different approaches. The methods and the codes used for the three objects in both cases are the same, to facilitate a reliable comparison. We analyze the bright SN 2012aw (Dall’Ora et al. 2014), the low-luminosity SN 2012A (Tomasella et al. 2013) and SN 2012ec. Several observational and derived parameters have been compared for these three objects. SN 2012aw ($M_R = -17.1$ mag, at plateau) is brighter than SN 2012ec ($M_R = -16.7$ mag), while SN 2012A is fainter ($M_R = -16.2$ mag). A comparison between the bolometric light curves shows that SN 2012ec has an intermediate luminosity between the high luminosity SN 2012aw and the fainter SN 2012A. The nickel mass synthesized by these SNe is $M(^{56}\text{Ni})_{12aw} = 0.056 \pm 0.013 M_\odot$, $M(^{56}\text{Ni})_{12ec} = 0.040 \pm 0.015 M_\odot$ and $M(^{56}\text{Ni})_{12A} = 0.011 \pm 0.004 M_\odot$. A spectroscopic comparison shows a similar time evolution at all epochs. The velocities of H_α , H_β and Fe II of SN 2012ec, place it in the middle of the higher velocities from SN 2012aw and the slowest SN 2012A at all times. The temperatures estimated are comparable for the three objects within the first 20 days, rather SN 2012ec tend to be similar to SN 2012A and they both are hotter than SN 2012aw. SN 2012aw has a more energetic explosion ($E = 1.5 \text{ foe}$) than SN 2012ec and SN 2012A ($E = 0.48 \text{ foe}$), but SN 2012ec is also more energetic than SN 2012A. We finally compared the results of the direct detection of the progenitors of these three SNe with the masses estimated from the hydrodynamical modelling. The progenitor mass estimated for SN 2012aw from the pre-explosion images ($M = 13 - 16 M_\odot$) and from the hydrodynamical modeling ($M_{eject} = 20 M_\odot$) show that the two methods are not in good agreement and that SN 2012aw has a more massive progenitor than SN 2012ec, the last one having comparable ejecta mass with SN 2012A ($M = 8 - 15 M_\odot$, $M_{eject} = 12.5 M_\odot$). The estimated initial radius of SN 2012aw ($R = 3 \times 10^{13} \text{ cm}$) indi-

cate a larger progenitor than for SN 2012ec and SN 2012A ($R = 1.8 \times 10^{13} \text{ cm}$). The estimates of the initial radius from the hydrodynamical modelling for the three objects is lower than those from the pre-explosion images and seem to be too low for a RSG progenitor. This homogeneous analysis finds a substantial match, within the errors, of the mass of the progenitor obtained with the two methods, mitigating the discrepancy which was pointed out in previous works (Maguire et al. 2010). SN 2012ec, SN 2012aw and SN 2012A also follow the relation obtained by Hamuy & Pinto 2002. This fact, coupled with their high luminosity at UV wavelengths, make Type IIP SNe interesting probes observable with the next generation of telescopes up to high z .

10 ACKNOWLEDGEMENTS

We thank E. Cappellaro for the useful discussions.

C.B. thanks the IRAP PhD program for the financial support. The research of JRM is supported through a Royal Society Research Fellowship. A.G.-Y. is supported by an EU/FP7-ERC grant no [307260], "The Quantum Universe" I-Core program by the Israeli Committee for planning and budgeting and the ISF, GIF, Minerva, ISF and Weizmann-UK grants, and the Kimmel award. G.P. acknowledges partial support by proyecto interno UNAB DI-303-13/R. GP and MH acknowledge support provided by the Millennium Institute of Astrophysics (MAS) through grant IC120009 of the Programa Iniciativa Científica Milenio del Ministerio de Economía, Fomento y Turismo de Chile". M.D.V., M.L.P., S.B., A.P., L.T. and M.T. are partially supported by the PRIN-INAF 2011 with the project "Transient Universe: from ESO Large to PESSTO". This work was partly supported by the European Union FP7 programme through ERC grant number 320360.

This work is based (in part) on observations collected at the European Organisation for Astronomical Research in the Southern Hemisphere, Chile as part of PESSTO, (the Public ESO Spectroscopic Survey for Transient Objects Survey) ESO program 188.D-3003, 191.D-0935. The research leading to these results has received funding from the European Research Council under the European Union’s Seventh Framework Programme (FP7/2007-2013)/ERC Grant agreement n° [291222] (PI : S. J. Smartt) and STFC grants ST/I001123/1 and ST/L000709/1.

The early SN 2012ec data have been collected via the ESO-NTT Large Program Supernova Variety and Nucleosynthesis Yields (184.D-1140), an European supernova collaboration led by Stefano Benetti (<http://sngroup.oapd.inaf.it/esolarge.html>). This paper is partially based on observations collected at Copernico telescope (Asiago, Italy) of the INAF - Osservatorio Astronomico di Padova; at the Galileo 1.22m Telescope operated by Department of Physics and Astronomy of the University of Padova at Asiago; at the 2.56m Nordic Optical Telescope operated by The Nordic Optical Telescope Scientific Association (NOTSA); at the 4.3m William Herschel Telescope operated by the Isaac Newton Group of Telescopes; on observations obtained through the CNTAC proposal CN2012B-73 and on observations made with the Liverpool Telescope (programme OL12B) operated on the island of La Palma by Liverpool John Moores University in the Spanish Ob-

servatorio del Roque de los Muchachos of the Instituto de Astrofísica de Canarias with financial support from the UK Science and Technology Facilities Council.

REFERENCES

- Arcavi I., Gal-Yam A., Cenko S.B. et al., 2012, *APJ*, 756L, 30A
- Arnett W.D. & Fu A. 1989, *APJ*, 340, 396
- Barbon R., Ciatti F., & Rosino L., 1979, *A&A*, 72, 287
- Baron E., Nugent P.E., Branch D. et al., 2004, *APJ*, 616, L91
- Bayless A.J., Pritchard T.A., Roming P.J., et al., 2013, *APJ*, 764L, 13B
- Bersten M.C., Benvenuto O., Nomoto K. et al., 2012, *APJ*, 757, 31B
- Blinnikov S., Lundqvist P., Bartunov O., et al. 2000, *APJ*, 532, 1132B
- Botticella M.T., Trundle C., Pastorello A. et al., 2010, *ApJ*, 717L, 52B
- Bose S., Kumar B., Sutaria F. et al., 2013, *MNRAS*, 433, 1871B
- Botticella M.T., Smartt S.J., Kennicutt R.C. et al., 2012, *A&A*, 537A, 132B
- Bouchet P., Danziger I.J. & Lucy L.B. 1991, *AJ*, 102, 1135
- Cappellaro E., Evans R. & Turatto M. 1999, *A&A*, 351, 459
- Cardelli J.A., Clayton G.C. & Mathis J.S. 1989, *APJ*, 345, 245
- Carpenter J.M., 2001, *AJ*, 121, 2851
- Clocchiatti A., Benetti S., Wheeler J.C., et al. 1996, *AJ*, 111, 1286C
- Coppola G., Dall’Ora M., Ripepi V., et al. 2011, *MNRAS*, 416, 1056C
- Childress M., Scalzo R., Yuan F., Schimdt B., 2012, *Central Bureau Electronic Telegrams*, 3201, 2
- Chugai N.N., & Utrobin V.P., 2000, *A&A*, 354, 557C
- D’Andrea C.B., Sako M., Dilday B., et al. 2010, *APJ*, 708, 661D
- Dalhen T., Strolger L.G., Riess A.G., et al. 2012, *APJ*, 757, 70D
- Dall’Ora M., Botticella M.T., Pumo L., et al. 2014, *APJ*, 787, 139
- Eastman R.G., Schmidt B.P. & Kirshner R., 1996, *ApJ*, 466, 911E
- Eldridge J.J. & Tout C.A., 2004, *MNRAS*, 353, 87E
- Elmhamdi A., Danziger I.J., Chugai N. et al., 2003, *MNRAS*, 338, 939E
- Elmhamdi A., Chugai, & N. Danziger I.J., 2003, *A&A*, 404, 1077E
- Filippenko A.V., 1997, *ARA&A*, 35, 309
- Fraser M., Maund J.R., Smartt S.J., et al., 2012, *APJ*, 759L, 13F
- Freedman W.L., Madore B.F., Gibson B.K., et al., 2001, *APJ*, 553, 47F
- Gilmozzi R., Cassatella A., Clavel J., et al., 1987, *Nature*, 328, 318G
- Grassberg E.K., Imshennik V.S., Nadyozhin D.K., 1971, *Ap&SS*, 10, 28G
- Gustafsson B., Edvardsson B., Eriksson K., 2008, *A&A*, 486, 951G
- Hamuy M. et al., 2001, *APJ*, 566, L63
- Hamuy M. & Pinto P., 2002, *APJ*, 558, 615
- Harutyunyan A., Pfahler P., Pastorello A., 2008, *A&A*, 488, 383H
- Heger A., Fryer C.L., Woosley S.E., Langer N., & Hartmann D.H., 2003, *APJ*, 591, 288
- Hook I.M., 2013, *Royal Society of London Philosophical Transactions Series A*, 371, 20282
- Hopkins P.F., Somerville R.S., Hernquist L., et al., 2006, *APJ*, 652, 864H
- Iben I. & Renzini A., 1983, *ARA&A*, 21, 271
- Inserra C., Turatto M., Pastorello A. et al, 2011, *MNRAS*, 417, 261I
- Inserra C., Turatto M., Pastorello A. et al, 2012, *MNRAS*, 422, 1122
- Jerkstrand A., Fransson C., Maguire K. et al, 2012, *A&A*, 546A, 28J
- Jerkstrand A., Smartt S.J., Fraser M. et al, 2014, *MNRAS*, 439, 3694J
- Kasen D. & Woosley S.E., 2009, *APJ*, 703, 2205
- King J.Y., Modjaz M., Shefler T. et al, 1998, *IAUC*, 6992, 1
- Kirshner R.P. & Kwan J., 1974, *APJ*, 193, 27K
- Kirshner R.P., Sonneborn G., Crenshaw D.M., et al., 1987, *APJ*, 320, 602K
- Kochanek C.S., Khan R. & Dai X., 2012, *APJ*, 759, 20K
- Kowal C.T., 1968, *AJ*, 73, 1021K
- Landolt A.U., 1992, *AJ*, 104, 340L
- Leonard D.C. et al., 2002, *PASP*, 114, 35L
- Li W., Cenko S.B. & Filippenko A.V., 2009, *Central Bureau Electronic Telegrams*, 1656, 1
- Li W., Leaman J., Chornork R., et al., 2011, *MNRAS*, 412, 1441
- Litvinova I. Yu., Nadezhin D.K., 1983, *Ap&SS*, 89, 89L
- Litvinova I. Yu., Nadezhin D.K., 1985, *Pis’ma Astron. Zh.*, 11, 351
- Maguire K., et al. 2010, *MNRAS*, 404, 981
- Massey P., Waterhouse E. & DeGioia-Eastwood K., 2000, *AJ*, 119, 2214
- Massey P., DeGioia-Eastwood K. & Waterhouse E. 2001, *AJ*, 121, 1050
- Maund J.R., Fraser M., Smartt S.J., et al. 2013, *MNRAS*, 413L, 102M
- Mitchell R.C., Baron E., Branch D., et al. 2002, *ApJ*, 574, 293M
- Moiseev A.V., 2000, *A&A*, 363, 843M
- Monard L.A.G., 2012, *Central Bureau Electronic Telegrams*, 3201, 1
- Mould J.R., Huchra J.P., Freedman W.L., et al. 2000, *APJ*, 529, 786M
- Nakano S., Aoki M., Kushida Y. et al, 1996, *IAUC*, 6442, 1
- Nakano S., 2006, *CBET*, 470, 1N
- Nugent P., Sullivan M., Ellis R., et al. 2006, *APJ*, 645, 841
- Olivares E.F., Hamuy M., Pignata G., et al. 2010, *APJ*, 715, 833
- Pastorello A., Zampieri L., Turatto M., et al. 2004, *MNRAS*, 347, 74P
- Pastorello A., Valenti S., Zampieri L., et al. 2009, *MNRAS*, 394, 2266P
- Pastorello A., Crockett R.M., Martin R., et al. 2009, *A&A*, 500, 1013P

- Pastorello A., Pumo M.L., Navasardyan H., et al. 2012, A&A, 537A, 141P
- Perlmutter S., Aldering G., Goldhaber G., et al. 1999, APJ, 517, 565P
- Poznanski D., Butler N., Filippenko A.V., et al. 2009, APJ, 694, 1067
- Poznanski D., Prochaska J.X., & Bloom J.S. 2012, MNRAS, 426, 1465P
- Pumo M.L., Zampieri L. & Turatto M., 2010, MSAIS, 14, 123
- Pumo M.L. & Zampieri L., 2011, APJ, 741, 41
- Quimby R.M., Wheeler J.G., et al. 2007, APJ, 666, 1093
- Ramya S., Sahu D.K. & Prabhu T.P., et al. 2007, MNRAS, 381, 511
- Riess A.g., Filippenko A.V., Challis P., et al. 1998, AJ, 116, 1009R
- Riess A.G., Macri L., Casertano S., et al. 2011, APJ, 730, 119R
- Rizzi L., Tully R.B., Makarov D., et al. 2007, APJ, 661, 815R
- Roy R., Sutaria F., Bose S., et al. 2007, IAUS, 296, 116R
- Rubin D., Knop R.A., Rykoff E., et al. 2013, ApJ, 763, 35R
- Schlafly E.F. & Finkbeiner D.P., 2011, APJ, 737, 103
- Schmidt B.P., Kirshner R.P., Eastman R.G., 1994, APJ, 432, 42S
- Schmidt B.P., Suntzeff N.B., Phillips M.M., 1998, APJ, 507, 46S
- Skrutskie M.F., Cutri R.M., Stiening R., et al. 2006, AJ, 131, 1163
- Smartt S.J., 2009, ARA&A, 47, 63
- Smartt S.J., Eldridge J.J., Crockett R.M., 2009, MNRAS, 395, 1409S
- Smith J.A., Tucker D.L., Kent S., 2002, AJ, 123, 2121S
- Spiro S., Pastorello A., Pumo M.L., 2014, MNRAS, 439, 2873S
- Stetson P.B., 1987, PASP, 99, 191S
- Suntzeff N.B., Hamuy M., Martin G. et al., 1988, AJ, 96, 1864S
- Tammann G.A. & Reindl B., 2013, A&A, 549A, 136T
- Tomasella L., Cappellaro E., Fraser M., et al. 2013, MNRAS, 434, 1636T
- Tully R., Rizzi L., Shaya E.J., et al. 2009, AJ, 138, 323T
- Turatto M., Benetti S., Cappellaro E. 2003, in From Twilight to Highlight: The Physics of Supernovae, ed. W. Hillebrandt & B. Leibundgunt, 200
- Utrobin V.P., 1993, A&A, 281L, 89U
- Utrobin V.P., 2007, A&A, 461, 233U
- Utrobin V.P., Chugai N.N., Pastorello A. 2007, A&A, 475, 973U
- Utrobin V.P. & Chugai N.N., 2008, A&A, 491, 507U
- Utrobin V.P. & Chugai N.N., 2009, A&A, 506, 829U
- Valenti S., Fraser M., Benetti S., et al. 2011, MNRAS, 416, 3138
- Van Dyk S.D., Cenko S.B., Poznanski D., et al. 2012, APJ, 756, 131V
- Walmswell J.J. & Eldridge J.J., 2012, MNRAS, 419, 2054
- Weaver T.A., & Woosley S.E., 1980, AIPC, 63, 15W
- Woosley S.E., Heger A., & Weaver T.A. 2002, Rev. Mod. Phys., 74, 1015
- Yaron O., & Gal-Yam A. 2012, PASP, 124, 668Y
- Zampieri L., Shapiro S.L., Colpi M., et al. 1998, ApJ, 502L, 149Z
- Zampieri L., Pastorello A., Turatto M., et al. 2003, MNRAS, 338, 711
- Zampieri L., 2005, ASPC, 342, 358Z
- Zampieri L., 2007, AIPC, 924, 358Z